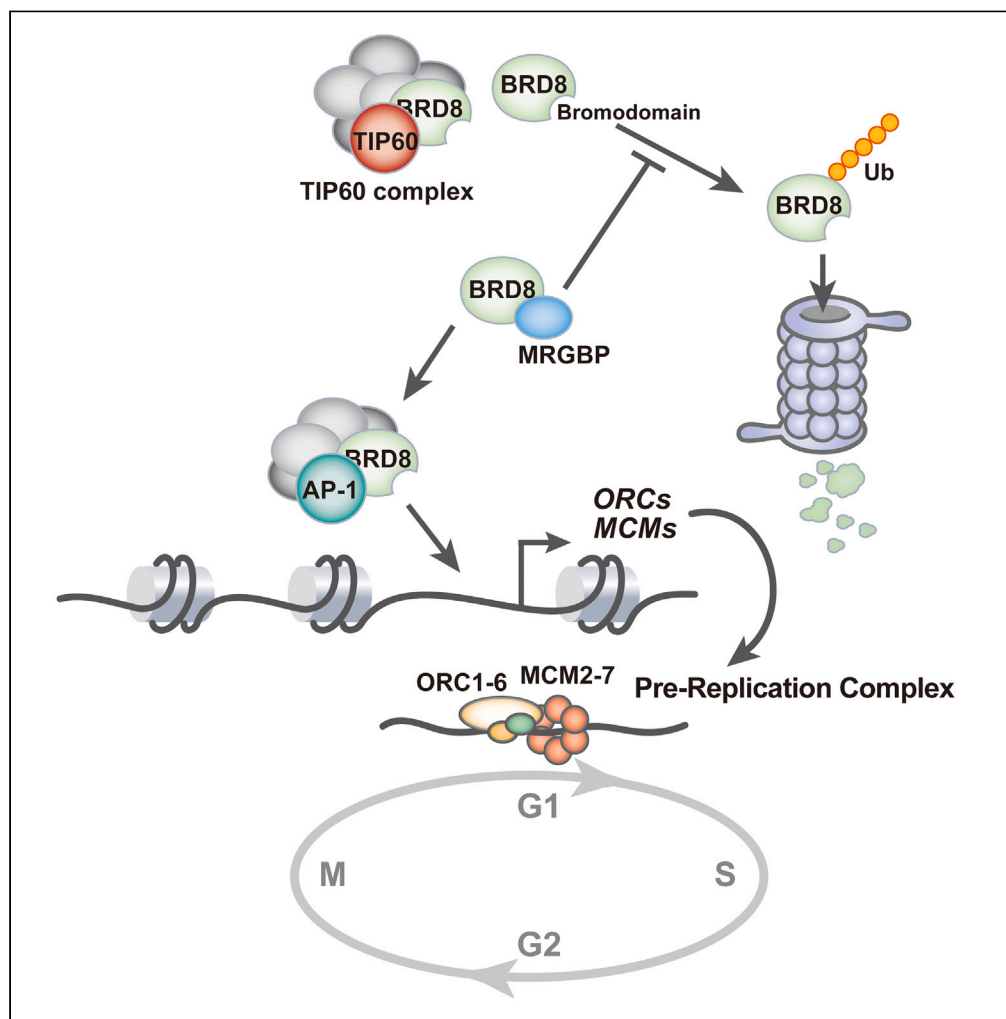## Article

Bromodomain protein BRD8 regulates cell cycle progression in colorectal cancer cells through a TIP60-independent regulation of the pre-RC complex

Kiyoshi Yamaguchi, Saya Nakagawa, Akari Saku, ..., Satoru Miyano, Seiya Imoto, Yoichi Furukawa

kiyamagu@g.ecc.u-tokyo.ac.jp (K.Y.)
yofurukawa@g.ecc.u-tokyo.ac.jp (Y.F.)

Highlights

Ubiquitin proteasome-dependent degradation of BRD8 is inhibited by MRGBP

BRD8 transactivates a set of genes independently of TIP60

BRD8 regulates the expression of multiple subunits of the pre-replicative complex

BRD8 is involved in the cell cycle progression and cell proliferation

iScience

Article

Bromodomain protein BRD8 regulates cell cycle progression in colorectal cancer cells through a TIP60-independent regulation of the pre-RC complex

Kiyoshi Yamaguchi,[1,10,]* Saya Nakagawa,[1] Akari Saku,[1] Yumiko Isobe,[1] Rui Yamaguchi,[2,3] Paul Sheridan,[4] Kiyoko Takane,[1] Tsuneo Ikenoue,[1] Chi Zhu,[1] Masashi Miura,[1] Yuya Okawara,[1] Satoru Nagatoishi,[5] Hiroko Kozuka-Hata,[6] Masaaki Oyama,[6] Susumu Aikou,[7] Yuka Ahiko,[7] Dai Shida,[7] Kouhei Tsumoto,[5,6,8] Satoru Miyano,[9] Seiya Imoto,[4] and Yoichi Furukawa[1,]*

SUMMARY

Bromodomain-containing protein 8 (BRD8) is a subunit of the NuA4/TIP60-histone acetyltransferase complex. Although BRD8 has been considered to act as a co-activator of the complex, its biological role remains to be elucidated. Here, we uncovered that BRD8 accumulates in colorectal cancer cells through the inhibition of ubiquitin-dependent protein degradation by the interaction with MRG domain binding protein. Transcriptome analysis coupled with genome-wide mapping of BRD8-binding sites disclosed that BRD8 transactivates a set of genes independently of TIP60, and that BRD8 regulates the expression of multiple subunits of the pre-replicative complex in concert with the activator protein-1. Depletion of BRD8 induced cell-cycle arrest at the G1 phase and suppressed cell proliferation. We have also shown that the bromodomain of BRD8 is indispensable for not only the interaction with histone H4 or transcriptional regulation but also its own protein stability. These findings highlight the importance of bromodomain as a therapeutic target.

INTRODUCTION

Disruption of normal histone modification patterns is frequently observed in cancer cells. Acetylation of lysine residues on histone tails plays an important role in the regulation of gene transcription.[1] Bromodomain proteins selectively recognize and bind to acetylated lysine residues, thereby participating in transcriptional regulation. The most extensively studied bromodomain protein is bromodomain-containing protein 4 (BRD4). Recent studies disclosed genetic alterations of *BRD4* including gene fusions and amplifications in squamous cell carcinoma[2,3] and ovarian carcinoma.[4] BRD4 governs the expression of genes including the c-Myc proto-oncogene through super-enhancers.[5,6] Importantly, studies on BRD4 provided the first proof-of-concept that bromodomain is a promising druggable target.[7] Indeed, JQ1, a pan-BET inhibitor, showed phenocopy of BRD4 knockdown and suppressed tumor growth *in vitro* and *in vivo*.[4,7]

We previously identified bromodomain-containing protein 8 (BRD8) as a protein that interacts with MRG domain binding protein (MRGBP)[8] that is frequently overexpressed in colorectal cancer (CRC)[9] and other types of cancer.[10–12] We also showed that this interaction results in stabilization of the BRD8 protein.[8] Reportedly, BRD8 and MRGBP are subunits of a multiprotein complex of TIP60 (Tat interacting protein, 60 kDa) histone acetyltransferase comprising at least 16 other subunits such as TRRAP, EP400, EPC1, ING3, MBTD1, MRG15, and MRGX.[13–15] Because BRD8 contains bromodomain(s), it is plausible to speculate that increased BRD8 expression enhances the transcription in concert with the TIP60 complex. Several reports suggested that TIP60 plays tumor-suppressive roles in certain types of cancer. For example, heterozygous mice bearing a null allele of *Tip60* showed an acceleration in tumorigenesis.[16] Tip60-mediated acetylation played a critical role in p53-dependent apoptotic response.[17] In contrast to these tumor suppressive roles of TIP60, BRD8 protein accumulates in metastatic colorectal cancer (CRC) cells[18] and reduced expression of BRD8 suppressed cancer cell proliferation *in vitro* and *in vivo*.[19,20] In addition, knockdown of BRD8 sensitized cytotoxic reagents to cancer cells.[18] These data suggested a tumor-promoting role of BRD8 in human carcinogenesis, which is inconsistent with the tumor-suppressive role of TIP60.

[1]Division of Clinical Genome Research, Advanced Clinical Research Center, The Institute of Medical Science, The University of Tokyo, Tokyo 108-8639, Japan

[2]Division of Cancer Systems Biology, Aichi Cancer Center Research Institute, Nagoya, Aichi 464-8681, Japan

[3]Division of Cancer Informatics, Nagoya University Graduate School of Medicine, Nagoya, Aichi 466-8550, Japan

[4]Division of Health Medical Intelligence, Human Genome Center, The Institute of Medical Science, The University of Tokyo, Tokyo 108-8639, Japan

[5]Project Division of Advanced Biopharmaceutical Science, The Institute of Medical Science, The University of Tokyo, Tokyo 108-8639, Japan

[6]Medical Proteomics Laboratory, The Institute of Medical Science, The University of Tokyo, Tokyo 108-8639, Japan

[7]Division of Frontier Surgery, Advanced Clinical Research Center, The Institute of Medical Science, The University of Tokyo, Tokyo 108-8639, Japan

[8]Department of Bioengineering, School of Engineering, The University of Tokyo, Tokyo 113-8656, Japan

[9]Department of Integrated Analytics, M&D Data Science Center, Tokyo Medical and Dental University, Tokyo 113-8510, Japan

[10]Lead contact

*Correspondence:
kiyamagu@g.ecc.u-tokyo.ac.jp (K.Y.),
yofurukawa@g.ecc.u-tokyo.ac.jp (Y.F.)

https://doi.org/10.1016/j.isci.2023.106563

In this study, we explored the target genes of BRD8 and TIP60 to identify their distinct roles in colorectal carcinogenesis and focused on downstream genes and cellular pathways that are not regulated by TIP60 but are regulated by BRD8. As a result, we found that BRD8 regulates multiple subunits of the pre-replication complex (pre-RC) in a TIP60-independent manner and that these genes play an important role in the regulation of the cell cycle. We also revealed that the bromodomain of BRD8 is indispensable for transcriptional regulation. These findings provide an insight into the roles played by MRGBP-BRD8 in human colorectal carcinogenesis and will contribute to the development of new chemotherapeutic agents targeting the bromodomain of BRD8.

RESULTS

Dominant expression of BRD8 isoform 1 in CRC cells

In the previous study, we showed that BRD8 protein was stabilized through the interaction with MRGBP in CRC cells. According to the databases, NCBI, UniProt, and Ensembl, BRD8 has at least four protein-coding isoforms. Among them, two major structural forms, isoform 1 ("GenBank: NP_006687") and isoform 2 ("GenBank: NP_631938"), are encoded by transcript variant 1 ("GenBank: NM_006696", "Ensembl: ENST00000230901") and variant 2 ("GenBank: NM_139199", "Ensembl: ENST00000254900"), respectively. In UniProt, isoform 1 and isoform 2 are swapped, i.e., isoform 1 ("GenBank: NP_006687") and isoform 2 ("GenBank: NP_631938") in NCBI correspond to "UniProtKB: Q9H0E9-2" and "UniProtKB: Q9H0E9-1" in UniProt, respectively. Differential exon usage of BRD8 variant transcript is illustrated in RNA-seq data of human tissues (GTEx, https://gtexportal.org/) (Figure S1A). Compared with isoform 1 comprising 951 amino acids, BRD8 isoform 2 comprising 1,235 amino acids lacks 73 amino acids in its central region and has a different C-terminal region. Both have bromodomain 1 (BD1), but only isoform 2 has an additional bromodomain (BD2) at the C-terminus. The expression of *BRD8* transcript variant 1 is relatively low in normal tissues, while variant 2 is abundantly and exclusively expressed in the testis (Figures S1A and S1B). Immunoblotting of BRD8 in CRC cell lines detected two bands above 150 kDa (Figures S2A and S2B). Comparison of the bands with isoform 1 and 2 proteins expressed exogenously in HEK293FT cells suggested that the band with the higher molecular weight corresponds to isoform 1 (Figure S2A). Another lower band may be a cleaved product of isoform 1. Consistent with our previous report, BRD8 and MRGBP were abundantly expressed in colorectal tumors compared with non-cancerous colonic mucosa (Figure S2C). Since these two bands were mainly detected in CRC tissues and cell lines, this study focused on the analysis of BRD8 isoform 1.

Association of the bromodomain of BRD8 with histone H4

Bromodomains were originally found in chromatin-associated proteins as an evolutionarily conserved motif,[21] and have been shown to be an effector module for acetyl-lysine binding.[22] Since BRD8 is a subunit of the TIP60 complex that preferentially acetylates histone H4,[23,24] interaction between BRD8 and histone H4 was evaluated using the NanoBRET protein-protein interaction assay.[25] BRD4 was parallelly tested as a positive control. Either the wild-type or the mutant NanoLuc-BRD4 (donor) was co-expressed with HaloTag-histone H4 (acceptor) in HCT116 cells and the signals were measured using filtered luminescence (Figure 1A). Combination of wild-type BRD4 and H4 significantly increased the ΔBRET ratio, and mutant BRD4 lacking the bromodomains in place of the wild-type almost reversed the activity to the baseline, suggesting that the bromodomains are substantially responsible for the interaction (Figure 1B). We then tested the interaction between NanoLuc-BRD8 (donor) and HaloTag-histone H4 (acceptor) in the cells. Wild-type of BRD8 increased ΔBRET ratio but the mutant BRD8 lacking the bromodomain significantly reduced the ratio, suggesting that the bromodomain is responsible for the interaction of BRD8 with H4. We additionally tested the effect of JQ1, a traditional pan-BET bromodomain inhibitor, on the interaction between the bromodomains and histone H4. Although treatment with JQ1 inhibited the interaction of histone H4 with wild-type BRD4, it did not affect the interaction with wild-type BRD8 (Figure 1C). This agrees with the result of phylogenic analysis which depicts bromodomains of BRD8 as a separated branch from other bromodomains (Figure 1D).

The bromodomain of BRD8 is essential for the interaction with MRGBP

To identify a responsible region of BRD8 for the interaction with MRGBP, we performed co-immunoprecipitation (Co-IP) using deletion mutants of BRD8 (Figure 2A). Although wild-type BRD8 bound to MRGBP, BRD8ΔB lacking the bromodomain and C-terminal residues failed to associate with MRGBP (Figure 2B). This interaction was observed when BRD8ΔC lacking only the C-terminal residues was used, suggesting that the bromodomain is an essential module for the interaction with MRGBP. A marked augmentation of the bromodomain-deletion mutant was also observed (Figure 2B, lane 5). Although we examined
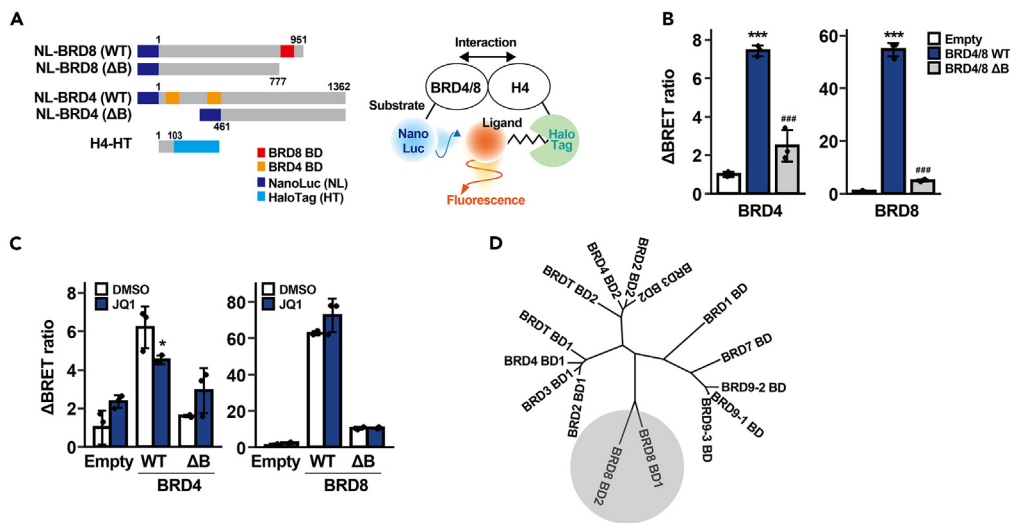
Figure 1. Bromodomain of BRD8 plays a role in the interaction with histone H4

(A) Schematic diagram illustrating wild-type and deletion mutants of BRD8 and BRD4 proteins used in this study. Schematic diagram showing energy transfer from a NanoLuc-BRDs fusion proteins (energy donor) to a fluorescently labeled HaloTag-histone H4 fusion protein (energy acceptor) upon interaction of BRD4/8 and histone H4. This system is a bioluminescence resonance energy transfer (BRET)-based assay and detects protein interactions by measuring energy transfer from a bioluminescent protein donor to a fluorescent protein acceptor in cells. NL, Nanoluc luciferase; HaloTag, modified haloalkane dehalogenase designed to covalently bind to synthetic ligands; BD, bromodomain.

(B) NanoBRET detected the interaction of H4 with BRD8 as well as BRD4. Data are presented as the mean ± SD of three independent cultures. Statistical significance was determined by Turkey's test. ***$p < 0.001$ vs. Empty. ###$p < 0.001$ vs. BRDs-WT.

(C) Treatment with JQ1 (500 nM) had no influence on the interaction between BRD8 and H4. Data are presented as the mean ± SD of three independent cultures. Statistical significance was determined by unpaired t-test. *$p < 0.05$ vs. DMSO.

(D) Phylogenetic analysis of bromodomains showing similarities of amino acid sequences.

whether MRGBP associates with BRD4, a well-studied bromodomain protein, MRGBP did neither interact with nor increase the BRD4 protein (Figure S2D). This result implies that the bromodomain of BRD8 contains a characteristic amino acid sequence required for the interaction with MRGBP.

Accumulation of BRD8 in the presence of MRGBP

Based on the functional features of bromodomains and the presence of a putative nuclear localization signal between codons 76 and 85 (with a score of 6.0) by cNLS Mapper (https://nls-mapper.iab.keio.ac.jp/cgi-bin/NLS_Mapper_form.cgi), BRD8 is thought to act in the nucleus. Immunocytochemical staining of wild-type BRD8 depicted its subcellular localization in the nucleus and cytoplasm, but mutant BRD8 protein lacking the NLS (BRD8ΔN) was restricted to the cytoplasm (Figures 2A and 2C). Using the plasmids expressing wild-type or mutant BRD8, we investigated the effect of MRGBP on the subcellular localization of BRD8. The expression of wild-type BRD8 was increased by MRGBP in both nuclear and cytoplasmic fractions (Figure 2D). Unexpectedly, BRD8ΔN accumulated not only in the cytoplasm but also in the nucleus. Thus, we re-analyzed BRD8 using cNLS Mapper with low cut-off values and found two additional NLSs, one between codons 94 and 125 (score 4.5) and the other between codons 118 and 150 (score 3.4). Another prediction tool, INSP (Identification of Nucleus Signal Peptide; at http://www.csbio.sjtu.edu.cn/bioinf/INSP/), predicted two different NLSs at codons 168–181 and 901–913. Therefore, these regions may act as additional NLSs and facilitate the nuclear transport of BRD8ΔN protein in the absence of the NLS at codons 76–85. Notably, BRD8ΔNB lacking both the NLS and bromodomain was dramatically increased in the cytoplasm even in the absence of MRGBP, suggesting that the bromodomain is mainly responsible for the destabilization or degradation of the BRD8 protein.

Degradation of BRD8 through ubiquitin-proteasome pathway

Since MRGBP-induced BRD8 expression occurs at the post-translational level,[8] we questioned whether MRGBP affects the stability of BRD8 protein. Cycloheximide chase assay revealed that wild-type BRD8
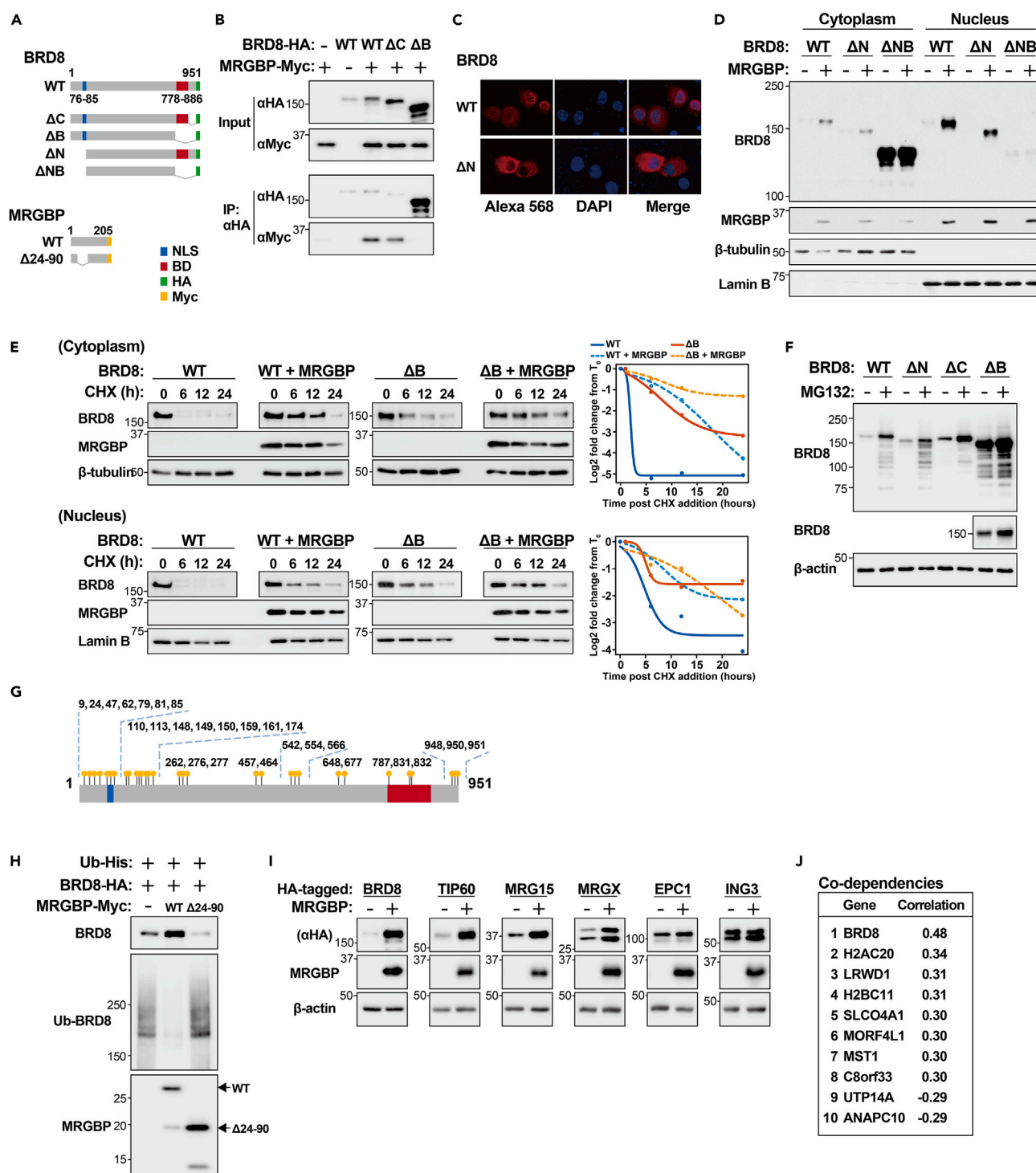
Figure 2. Stabilization of BRD8 protein by MRGBP

(A) Schematic diagram illustrating wild-type and deletion mutants of BRD8 and MRGBP proteins used in this study. NLS, nuclear localization signal; BD, bromodomain; HA, hemagglutinin epitope tag; Myc, c-Myc epitope tag.

(B) HEK293FT cells were transfected with Myc-tagged MRGBP and/or HA-tagged BRD8. Immunoprecipitation (IP) followed by immunoblotting showed that BRD8 interacts with MRGBP through the bromodomain.

(C) Immunocytochemical staining of wild-type and mutant BRD8 in COS-7 cells. Alexa 568, BRD8; DAPI, nuclei.

Figure 2. Continued

(D) The effect of MRGBP on the expression and subcellular localization of wild-type and mutant BRD8. β-Tubulin, a marker for the cytoplasmic fraction; Lamin B, a marker for the nuclear fraction.

(E) Protein samples were collected from HEK293FT cells expressing wild-type (WT) or mutant (ΔB) BRD8 in the presence or absence of MRGBP at the indicated time points after treatment with 100 μg/mL of cycloheximide (CHX). Representative immunoblotting using anti-HA and anti-Flag antibodies to detect BRD8 and MRGBP, respectively (left panel). Plots of the relative levels of BRD8 after CHX treatment (right panel). Levels of BRD8 are shown as the log2 transformed ratio relative to time 0. Data are presented as the mean of two-independent cultures. See also Figure S2E.

(F) The effect of MG132 proteasome inhibitor (10 μM, 8 h) on the expression of BRD8 in HEK293FT cells. Expression of β-actin served as an internal control.

(G) BRD8 ubiquitination sites identified by mass spectrometry. See also Table S1.

(H) Reduced ubiquitination of BRD8 by the co-expression of MRGBP, but not by mutant MRGBP (Δ24–90) which cannot bind BRD8.

(I) The effect of MRGBP on the expression of six subunits of the TIP60 complex. HEK293FT cells were transfected with the indicated plasmids, and the lysates were used for immunoblotting.

(J) Top 10 correlated genes from the data of MRGBP-dependency score (Pearson correlation). See also Figure S2H and Table S2.

underwent rapid proteolysis, and that co-expression of MRGBP markedly augmented both cytoplasmic and nuclear BRD8 (Figures 2E and S2E). Compared with wild-type BRD8, the degradation of BRD8ΔB protein was markedly retarded in the cytoplasm and nucleus without MRGBP. Co-expression of MRGBP slightly increased the stability in the cytoplasm.

Next, we examined BRD8 expression in the presence and absence of a proteasomal inhibitor MG132. Treatment with MG132 increased wild-type and two forms of mutant BRD8 (ΔN and ΔC) proteins, suggesting the involvement of the ubiquitin-proteasome pathway in BRD8 degradation. (Figure 2F). Importantly, BRD8ΔB remarkably accumulated even in the absence of MG132, and its accumulation was further enhanced by MG132. On the other hand, the bromodomain alone (BRD8-B) was increased by co-expression of MRGBP, whereas BRD8-B was not affected by MG132 (Figure S2F). These data suggest that the bromodomain plays an important role in the stabilization of BRD8 through the interaction with MRGBP and that the region outside of the domain is involved in its degradation by the ubiquitin-proteasome system.

To address the ubiquitination sites, we enriched peptides with ubiquitin remnant motif (K-ɛ-GG) using an anti-ubiquitin remnant motif antibody and performed mass spectrometry analysis. The proteomic analysis identified a total of 31 ubiquitination sites which were widely distributed in the BRD8 protein (Figure 2G and Table S1). To investigate whether MRGBP affects the ubiquitination of BRD8, we conducted a cell-based ubiquitination assay. As shown in Figure 2H, the ubiquitination of BRD8 was almost diminished by wild-type MRGBP, but not by mutant MRGBP (Δ24–90) which lacks the ability to bind BRD8.[8] Therefore, the ubiquitination of BRD8 may be interfered by the physical interaction of MRGBP with the bromodomain, which results in the stabilization of BRD8 (Figure S2G). Although the precise mechanism of BRD8 degradation needs further investigation, the interaction of the bromodomain with MRGBP may hamper the ubiquitination of BRD8 outside of the domain.

Effect of MRGBP on the components of the TIP60 complex

Although we and another group revealed that BRD8, MRG15, and MRGX, three subunits of the TIP60 complex, were increased by MRGBP,[8,26] the effect of MRGBP on the other subunits remains unclear. We focused on subunits that are essential for the acetyltransferase activity (TIP60, EPC1, and ING3)[14] and investigated their protein levels. In addition to BRD8, MRG15, and MRGX proteins, TIP60 protein was markedly augmented by MRGBP (Figure 2I). Since these results urged a functional inconsistency that MRGBP up-regulates both an oncogenic player of BRD8 and a tumor suppressor of TIP60, we explored genes that have a codependent relationship with MRGBP using the Cancer Dependency Map (DepMap), a database including genome-scaled pooled loss-of-function screening data (https://depmap.org/).[27] We found that MRGBP had the strongest codependency with BRD8 (score = 0.48) and moderate to weak codependency with MRG15 (0.30), EP400 (0.25), ING3 (0.22), EPC1 (0.20), and MEAF6 (0.15) (Figures 2J and S2H and Table S2). However, TIP60 was not included in the top 100 genes codependent with MRGBP or BRD8. These data suggested that TIP60 is not associated with MRGBP or BRD8, at least in cell survival.

Differentially expressed genes by the knockdown of BRD8 or TIP60

To explore the TIP60-dependent and TIP60-independent roles of BRD8 in CRC cells, we performed RNA-seq using HCT116 and SW480 cells transfected with BRD8 siRNAs (BRD8-KD) or TIP60 siRNAs (TIP60-KD) (Figure 3A). Differentially expressed gene analysis identified subsets of genes that were up- (460 genes) and down-regulated (590 genes) in BRD8-KD, and that were up- (527 genes) and down-regulated (643 genes) in
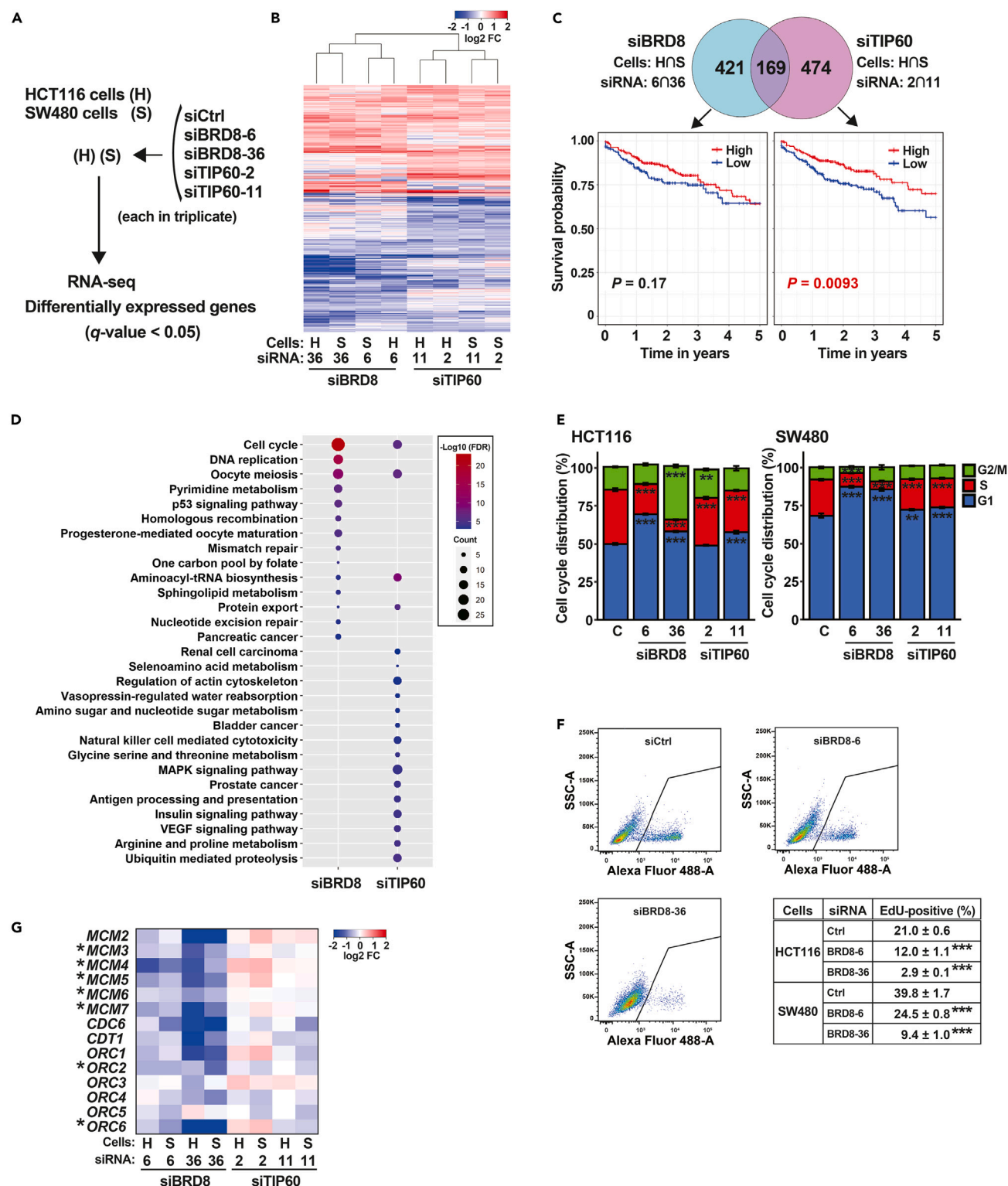
Figure 3. Comparisons of differentially expressed genes (DEGs) between in BRD8-KD and in TIP60-KD CRC cells

(A) Flowchart of RNA-seq. Two different CRC cells and siRNAs targeting BRD8 and TIP60 were used for the analysis. Each group was analyzed in triplicate.

(B) Heatmap of DEGs. The values represent log2 fold change (FC) of the gene expression in BRD8-KD and TIP60-KD groups relative to control siRNA group. See also Table S3.

Figure 3. Continued

(C) The number of genes significantly down-regulated by BRD8-KD and TIP60-KD. Kaplan-Meier survival curves for the 453 patients (TCGA-COAD), with classification based on the expression levels of coherent genes in each group. The generalized log rank test was used to compare the survival curves between the two groups. See also Figure S5.

(D) KEGG pathways significantly associated with down-regulated genes by BRD8-KD and TIP60-KD (FDR q-value <0.01). See also Table S4.

(E and F) Flow cytofluorometric analysis of cell cycle distributions using propidium iodide (E) and EdU incorporation (F). Data are presented as the mean $\pm$ SD of three independent cultures. Statistical significance was determined by Dunnett's test. **$p < 0.01$, ***$p < 0.001$ vs. siCtrl. See also Figure S4B.

(G) The expression values of the pre-RC subunits were extracted from the RNA-seq data. Asterisks represent a significant down-regulation in all BRD8-KD conditions.

H, HCT116 cells; S, SW480 cells

TIP60-KD cells (Figures 3B, 3C, and S3 and Table S3). A total of 169 genes were commonly down-regulated by the silencing of BRD8 or TIP60.

To understand the biological significance of BRD8 and TIP60 in colorectal carcinogenesis, we performed enrichment analysis using the list of genes down-regulated by BRD8-KD and TIP60-KD (https://www.gsea-msigdb.org/gsea/msigdb). The down-regulated genes were significantly enriched in 29 different Kyoto Encyclopedia of Genes and Genomes (KEGG) pathways including 14 in BRD8-KD and 19 in TIP60-KD (FDR q-values <0.01, Table S4). Although four pathways were shared by BRD8 and TIP60, the majority of the significant pathways associated with BRD8 and TIP60 were different (Figure 3D). It is of note that the "DNA replication" signature was highly specific to BRD8-KD. In gene ontology (GO) analysis, "cell cycle" is likely responsible for the most biological significance of BRD8 but not TIP60 (Figure S4A and Table S4).

To explore the clinical relevance of these gene sets, we performed extraction-of-expression modules (EEM) analysis, which tests the functionality of the input gene sets according to their coherence.[28] This analysis combined with the expression dataset in The Cancer Genome Atlas (TCGA) colonic adenocarcinoma (TCGA-COAD, n = 456) (Figure S5A) found that each gene set had a coherently expressed subset (Figure S5B). By merging their prognostic information (TCGA-COAD, n = 453), we found that patients with higher coherent gene subsets in the TIP60 group had a significantly better prognosis (p = 0.0093), whereas there was no difference in the BRD8 group (p = 0.17) (Figure 3C). This result is consistent with previous studies showing a tumor-suppressive role of TIP60.[16,17,29]

The effect of BRD8 and TIP60 on cell cycle progression

To confirm the role of BRD8 suspected from the differentially regulated genes, we examined the effects of BRD8-KD and TIP60-KD on cell cycle progression in HCT116 and SW480 cells. BRD8-KD significantly decreased the S population and increased the G1 population compared to the cells treated with control siRNA, suggesting a cell-cycle arrest at the G1/S boundary (Figure 3E). EdU incorporation assay showed that the knockdown of BRD8 significantly reduced the rate of DNA synthesis in both HCT116 and SW480 cells (Figure 3F). On the other hand, TIP60-KD significantly reduced the S population but the reduction was small compared with BRD8-KD. Similar results were observed in other methods using cells without ethanol fixation and dye with high membrane permeability and high specificity for DNA (Figure S4B). These data suggested that TIP60 may exert a limited impact on cell cycle progression.

Identification of genes encoding subunits of the pre-RC as direct targets of BRD8

Although the pathway analysis linked both BRD8 and TIP60 to "cell cycle" (Figure 3D), the knockdown of BRD8 and TIP60 showed different effects on the cell cycle. Thus, we compared cell cycle-associated genes regulated by BRD8-KD and TIP60-KD (Figure S4C) and found that the expression of *MCM3–7*, members of the minichromosome maintenance (MCM) protein complex, and *ORC2* and *ORC6*, components of the origin recognition complex (ORC), were reduced by BRD8-KD alone (Figure 3G). The TCGA data support that *MRGBP* expression was significantly correlated with *ORC2*, *ORC6*, *MCM3*, *MCM4*, and *MCM7* expression in colorectal adenocarcinoma tissues (Figure S4D). The *MCM* and *ORC* genes are components of the pre-replication complex (pre-RC) that forms at replication origins in the G1 phase, and this process is known as origin licensing. They are critically required for the assembly of the pre-RC, thereby leading to a possible link between BRD8 and "DNA replication" or "cell cycle" (Table S4).

We further explored genomic BRD8-binding sites across the human genome to identify target genes directly regulated by BRD8 (Figures S6A–S6D). ChIP-seq analysis of BRD8 detected a total of 5,287 significant peaks, and the vast majority of the peaks (77.9%) were located close to transcription start sites (TSS) of
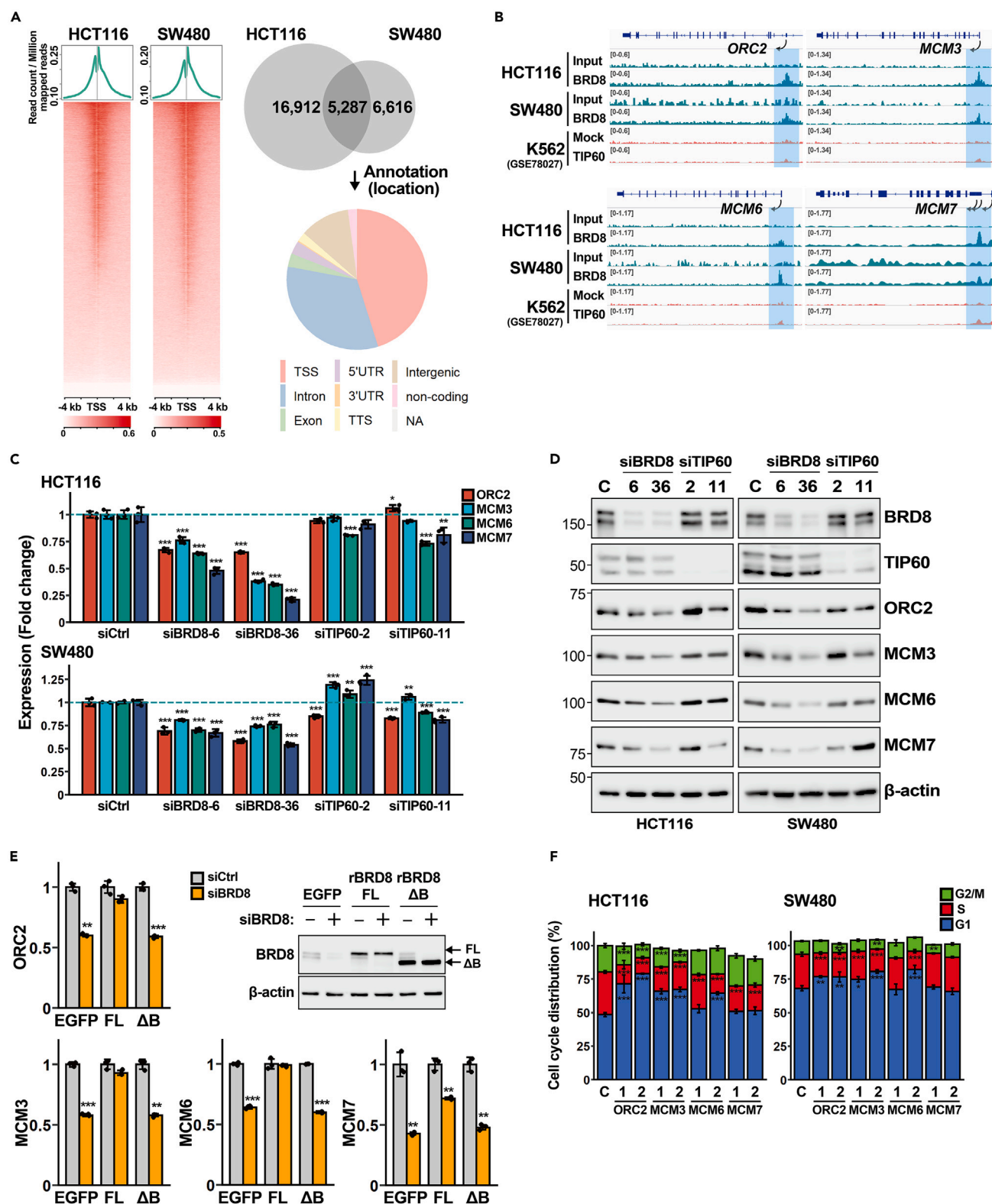
Figure 4. Genome-wide BRD8 binding profiling by ChIP-seq

(A) Heatmaps of distribution in BRD8-bound regions located within 4 kb of annotated TSSs. Venn diagrams depicting the number of overlapping BRD8 peaks from the two CRC cells. Pie chart of BRD8-binding sites relative to nearest gene. See also Figure S6 and Table S5.

Figure 4. Continued

(B) Visualization of peaks from BRD8 and TIP60 ChIP-seq data (GSE78027).

(C and D) Validation of reduced expression of the pre-RC subunits by the BRD8-KD using RT-qPCR (C) and immunoblotting (D). Data are presented as the mean ± SD of three independent experiments.

(E) HCT116 cells expressing EGFP, siBRD8-resisntant BRD8 (rBRD8-FL), or its bromodomain-lacking mutant (rBRD8-ΔB) were transfected with siCtrl or siBRD8-6. The expression of *ORC2* and *MCMs* were analyzed by RT-qPCR. Data are presented as the mean ± SD of three independent experiments.

(F) Cell cycle distributions in HCT116 and SW480 cells following knockdown of ORC2 and MCMs by siRNAs. Data are presented as the mean ± SD of three independent cultures. Statistical significance was determined by unpaired *t*-test (E) or Dunnett's test (C and F). *$p < 0.05$, **$p < 0.01$, ***$p < 0.001$ vs. siCtrl. See also Figure S7C.

genes and intronic regions (Figure 4A). Integrated analysis of the 421 down-regulated genes obtained from the RNA-seq (Figure 3C) and the BRD8-binding sites identified 193 potential direct targets of BRD8 (Table S5 and Figure S7A). In addition, we compared the ChIP-seq data of BRD8 and that of TIP60 (GSE78027)[15] containing a total of 637 significant TIP60-peaks (Table S6), of which 144 (22.6%) were not shared with BRD8-peaks. Although *ORC2*, *MCM3*, *MCM6*, and *MCM7* encoding four subunits of the pre-RC were included in the list of the 193 genes with BRD8-peaks, they were not included in TIP60 peaks (Figures 4B and S7B). In addition, the expression of ORC2, MCM3, MCM6, and MCM7 was not reduced by the TIP60-KD, indicating that their expression is regulated independently of TIP60 (Figures 4C and 4D).

To confirm the involvement of bromodomain in the regulation of the four genes, we generated BRD8 plasmids that are resistant to the BRD8 siRNA by introducing synonymous mutation at the target site. Immunoblotting showed that exogenous expression of full-length and mutant BRD8 lacking the bromodomain (rBRD8-FL and rBRD8-ΔB) was totally unaffected by the siRNA. The introduction of rBRD8-FL counteracted RNAi effects on the expression of *ORC2*, *MCM3*, *MCM6*, and *MCM7*, whereas rBRD8-ΔB did not affect their expression (Figure 4E). These data corroborated that bromodomain is indispensable for the regulation of these target genes.

In addition, analysis of these four genes on cell cycle progression revealed that knockdown of ORC2 and MCM3, but not MCM6 or MCM7, induced G1 arrest in the cells (Figures 4F and S7C). Although further analysis is necessary, ORC and MCM proteins including ORC2 and MCM3 may play a vital role in cell cycle progression, at least in part, as downstream genes of BRD8.

Involvement of AP-1 in the regulation of pre-RC subunits by BRD8

In addition to TIP60,[30] BRD8 has been reported to act as a co-activator of nuclear receptors including thyroid hormone receptor, 9-cis-retinoic acid receptor, and androgen receptor.[31–33] However, involvement of BRD8 in the regulation of other transcription factors (TFs) remains to be elucidated. To gain insight into the TIP60-independent transcriptional regulation, we searched for TF motifs enriched in the BRD8 binding regions. Although a broad range of TF motifs was enriched in the BRD8-peaks, a comparison of the motifs with those in TIP60-peaks discovered that motifs of FOS, FOSL1, FOSL2, JUN, and JUNB, members of AP-1 family were exclusively enriched in the BRD8-peaks (Figure 5A and Table S7). To see whether these AP-1 family members are involved in the regulation of BRD8 target genes, we suppressed the expression of FOS, FOSL1, FOSL2, JUN, or JUNB, and performed qPCR and cell cycle analyses (Figure S7D). The four pre-RC genes (*ORC2*, *MCM3*, *MCM6*, and *MCM7*) were consistently reduced by FOS-KD, FOSL1-KD, and FOSL2-KD in HCT116 cells (Figure 5B). Cell cycle analysis showed that the siRNA against FOS, FOSL1, and FOSL2 induced G1 arrest and reduced the S phase in SW480 cells (Figure 5C). On the other hand, JUN and JUNB siRNAs did not decrease the expression of *ORC2* nor arrest the G1 phase in the cells, suggesting that AP-1 proteins, especially FOS family members are relevant to the regulation of gene expression and cell cycle progression in concert with BRD8. Furthermore, Co-IP using anti-FOS, FOSL1, and FOSL2 antibodies uncovered that FOSL1 interacted with endogenous BRD8 in HCT116 cells (Figure 5D). In addition, FOSL1 co-precipitated with BRD8, but not with TIP60, in SW480 cells (Figure 5E). Therefore, BRD8 may interact with member(s) of the AP-1 family and induce downstream genes that are implicated in the progression of the cell cycle. Future studies will elucidate the precise mechanisms of cell cycle progression through the regulation of pre-RC components by BRD8.

BRD8 is implicated in cell proliferation *in vitro* and *in vivo*

Given that BRD8-KD induced cell-cycle arrest in CRC cells, we investigated the effect of BRD8-KD on cell proliferation using six CRC cell lines, namely HCT116, SW480, HT-29, LoVo, LS174T, and SW48. BRD8 siRNAs significantly reduced the proliferation of these cells in both 2D monolayer and 3D low-attachment cultures (Figures 5F and S7E). To confirm the suppressive effects of BRD8-KD on cell proliferation, we generated
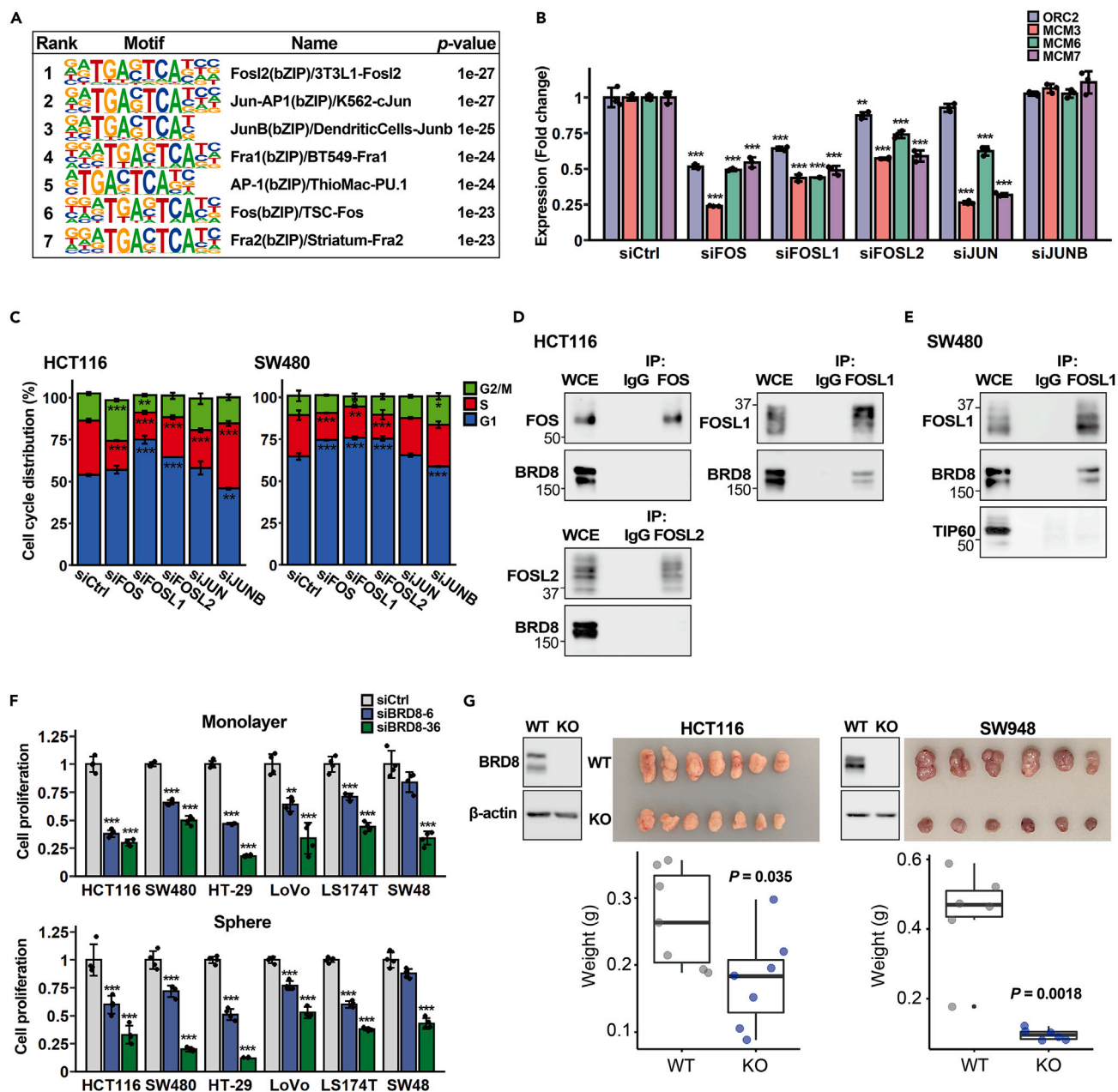
Figure 5. AP-1 is a novel binding partner of BRD8

(A) Co-occurrence of motifs in BRD8 peaks. BRD8-specific motifs were obtained by subtracting motifs in TIP60 peaks (Table S7). Top seven motifs were activator protein-1 (AP-1) family transcription factors.

(B) The effects of FOS/JUN members on the expression of pre-RC genes were evaluated by RT-qPCR. See also Figure S7D.

(C) Cell cycle distributions in HCT116 and SW480 cells transfected with siRNAs against the members of the FOS and JUN families.

(D) Interactions between endogenous BRD8 and FOS family members were assessed by immunoprecipitation (IP) using the indicated antibodies.

(E) BRD8, but not TIP60, was co-precipitated with FOSL1.

(F) Viability of CRC cells transfected with siBRD8s in monolayer and low-attachment sphere cultures. See also Figure S7E.

(G) BRD8-null HCT116 cells and SW948 cells were inoculated subcutaneously into nude mice (n = 6 or 7). Tumor weight was measured after 27 days. Statistical significance was determined by unpaired t-test. Unless specified otherwise, data are presented as the mean $\pm$ SD of three or four independent cultures. Statistical significance was determined by Dunnett's test. *p < 0.05, **p < 0.01, ***p < 0.001 vs. siCtrl. See also Figure S8.

BRD8-knockout HCT116 and SW948 cells (Figures S8A and S8B). In agreement with the results of *in vitro* cell proliferation, knockout of BRD8 significantly decreased tumor growth in the xenograft model (Figure 5G).

DISCUSSION

In this study, we have revealed that the bromodomain in BRD8 plays a key role in the interaction not only with histone H4 but also with MRGBP. In addition, we discovered that the binding with MRGBP results in the stabilization of the BRD8 protein by the suppression of ubiquitin-dependent proteasomal degradation, and that accumulated BRD8 is associated with cell cycle progression and proliferation of cancer cells through the TIP60-independent regulation of genes encoding multiple subunits of the pre-RC complex.

We carefully compared two major isoforms because recent studies disclosed the paradoxical role of BRD4 isoforms in breast cancer.[34] The oncogenic role of BRD4 is well accepted, but its long form exhibits tumor suppressive functions. It has been reported that BRD8 isoform 2 is up-regulated through the loss of miR-185 in prostate cancer and that it activates androgen receptor-mediated transcription.[31,35] However, BRD8 isoform 2 is expressed exclusively in the testis according to the gene expression database of multiple normal tissues (Figure S1). Although BRD8 isoform 1 is abundantly expressed in CRCs, the expression of BRD8 isoform 2 is not detected by immunoblotting (Figures S2A–S2C). Therefore, elevated MRGBP expression is likely to induce BRD8 isoform 1 but not isoform 2 in CRC cells.

Lashgari and colleagues reported that BRD8-KD leads to the induction of p53 and its target genes including *Fas*, *p21* (*CDKN1A*), *Puma* (*BBC3*), *TP53INP1*, *TIGAR*, and concomitant cell-cycle arrest in G1/S in HCT116 cells.[19] However, our data strongly suggested that BRD8 regulates cell cycle in a p53-independent manner because BRD8-KD retarded G1/S transition in SW480 cells carrying mutations in *TP53* (Figures 3E and S4B). In addition, BRD8 silencing using two different siRNAs did not consistently increase the expression of *TP53* and the target genes in our data (Table S3). In the cell cycle analysis, we found an unusual increase in the G2/M phase in HCT116 cells treated with siBRD8-36 (Figures 3E and S4B). However, BRD8 silencing using additional siBRD8-7 did not increase the G2/M cell population of HCT116 (Figure S7F). Immunoblot analysis also showed that siBRD8-36 remarkably induced p53 protein in HCT116 but not in SW480 and LS174T cells (Figure S7G). Since the induction of p53 increases the fraction of the G2/M phase in HCT116 cells,[36] the G2/M arrest observed in a certain condition may be caused by the off-target effect of siBRD8-36. Moreover, we confirmed the p53-independent regulation of cell cycle using p53-null HCT116 cells (Figure S7H).

During late M to G1 phase, the origin recognition complex (ORC) consisting of six subunits (ORC1–6) is known to bind to replication origins, which are then licensed by stably binding to the complex of MCM proteins (MCM2–7). The expression of *MCMs* is transcriptionally activated by E2F transcription factors as a part of the normal process of cell division,[37] and the complex is thought to function as a replicative helicase.[38] RNAi-mediated knockdown of MCM4–7 suppressed proliferation of HeLa cells without impairing DNA replication.[39] Although MCM3 siRNA barely affected the proliferation, cells with reduced concentration of MCM3 caused chromosomal instability and became hypersensitive to DNA replication stress. It has been reported that functional ablation of individual pre-RC proteins showed different phenotypes including cell cycle and cell death.[40] In line with the previous observations, our data also showed that the silencing effects of each subunit on cell cycle were inconsistent (Figure 4F). This may be explained by the different roles of MCM subunits from the initiation of DNA replication.[39,41] For example, MCM5 is involved in Stat1-mediated transcription,[42] and MCM7 interacts with Rad17 and is required for the recruitment of ATR to damaged DNA.[41] It has been unclear for a long time why cells produce a large excess of MCM2–7 relative to the number of replication forks. A recent study revealed that the surplus of MCMs increases the robustness of genome duplication by restraining the replication fork speed.[43] Conversely, limited licensing conditions such as low levels of MCMs accelerate replication forks and cause DNA damage. Since BRD8-KD decreased the expression of MCM3–7, elevated expression of MRGBP may accumulate nuclear MCM proteins through a BRD8-mediated transcriptional activation.

It has been reported that MCM3–7 undergo rapid degradation in the cytoplasm, and their stabilization and nuclear translocation require interaction with MCM-binding protein (MCMBP).[43] Therefore, although MCMBP is not involved in replication origins, it safeguards replicating genomes by increasing chromatin coverage with pre-RCs. Interestingly, we found that knockdown of BRD8 repressed MCMBP expression in addition to ORC/MCM (Table S3 and Figure S7I), suggesting that BRD8 may regulate not only the expression of MCMs but also their localization. Importantly, low levels of MCMs sensitize cancer cells to

replicative inhibitors by increasing endogenous replicating stress.[39,43] Reportedly, silencing of MCM2 or MCM3 resulted in the down-regulation of sensor proteins associated with DNA damage response, including H2AX, CHK1, and CHK2, suggesting that expression of these MCMs is relevant to the responses.[44] Consistent with this report, we found that knockdown of BRD8 reduced the phosphorylation of H2AX and RPA32 in HCT116 cells treated with camptothecin or doxorubicin (Figure S7J). The decreased activity of H2AX may have resulted from the reduced expression of MCMs by the knockdown of BRD8.

Bromodomain containing 9 (BRD9) is a key component of the SWI/SNF chromatin remodeling complex, known for its ability to recognize acetyl-lysine and their diverse roles in physiology and oncology.[45] Recently, a study of the target profiling of BRD9 probe, BI-9564, found unexpected off-target binding to BRD8.[46] Further efforts developed an improved BRD8 probe, DN01, showing 12 nM IC_{50} in AlphaScreen assay, with high selectivity over BRD9 (IC_{50}: 10 μM) and BRD4 (IC_{50}: >10 μM). It is intriguing to test whether DN01 alters the expression of pre-RC subunits. Combined application of BRD8 inhibitors with DNA damaging agents may be an effective therapeutic approach to treat human cancer.

Our findings provide evidence that bromodomain is the key for the determination of BRD8 function. Furthermore, our data support the notion that inhibitors of BRD8 may suppress the growth of cancer cells and sensitize them to DNA-damaging agents. Identification of chemical probes that interfere with the association between BRD8 and histone H4 using NanoBRET assay may facilitate the development of effective anticancer drugs for the treatment of CRC.

Limitations of the study

Considering the roles of bromodomain in gene transcription, BRD8 is anticipated to enhance transcriptional activation, which is likely to represent significant biological roles of BRD8. Meanwhile, down-regulated genes by BRD8 might also contribute to its biological roles. In lung epithelial cells, BRD8-KD induced the expression of *DEFB1*, *CCL5*, and *CXCL6*.[47] Since these genes encode antimicrobial protein and chemokines, BRD8 may be involved in the suppression of immune responses in the mucosal barrier in the airway epithelium. However, these genes were not up-regulated in our data obtained from the BRD8-KD CRC cells (Table S3). Consistently, immune response or its equivalents was not included in GO terms or KEGG pathways associated with the up-regulated genes in BRD8-KD CRC cells, suggesting that BRD8 exhibits cell type-dependent gene regulation (Figures S3C and S4A). In addition, we found a significant increase in the expression of AXIN2 in response to the BRD8-KD (Table S3 and Figure S3D). Because Axin2 acts as a scaffold protein in the β-catenin destruction complex,[48] increased Axin2 expression suppresses β-catenin/TCF-dependent transcription.[49] However, BRD8-KD did not change the activity of TOPflash reporter.[50] Further investigation into the biological consequences of Axin2 up-regulation by BRD8-KD in CRC cells will be essential (Figure S3E).

In this study, we have revealed different downstream genes and biological roles of BRD8 from TIP60, although both proteins are regulated by MRGBP. However, the precise regulatory mechanism of BRD8 by MRGBP and the functional interaction between BRD8 and AP-1 need investigating in future studies.

STAR★METHODS

Detailed methods are provided in the online version of this paper and include the following:

- KEY RESOURCES TABLE
- RESOURCE AVAILABILITY
  - Lead contact
  - Materials availability
  - Data and code availability
- EXPERIMENTAL MODEL AND SUBJECT DETAILS
  - Cell lines and culture conditions
  - Colorectal tumor tissues
  - Xenograft tumor in nude mice
- METHOD DETAILS
  - Gene silencing
  - Plasmids
  - Quantitative PCR (qPCR)
  - Construction of RNAi-resistant plasmids and rescue experiment

- ○ Flow cytometry
- ○ Cell viability assay
- ○ Immunocytochemical staining
- ○ Cycloheximide chase assay
- ○ Immunoblot analysis
- ○ Immunoprecipitation
- ○ Nuclear extraction
- ○ Cell-based ubiquitination assay
- ○ Identification of ubiquitination sites by mass spectrometry
- ○ NanoBRET PPI analysis
- ○ Reporter assay for measuring Wnt signaling activity
- ○ RNA-seq analysis
- ○ Over-representation analysis (ORA)
- ○ Extraction-of-expression modules analysis
- ○ ChIP-seq analysis
- ○ Establishment of BRD8-knockout cells
- ● QUANTIFICATION AND STATISTICAL ANALYSIS

AUTHOR CONTRIBUTIONS

Conceptualization, K.Y. and Y.F.; Methodology, R.Y., P.S., K.Ta., T.I., and S.N.; Formal Analysis, K.Y. and R.Y.; Investigation, K.Y., S.N., A.S., Y.I., C.Z., M.M., Y.O., and H.K-H.; Resources, S.A., Y.A., and D.S.; Visualization, K.Y. and R.Y.; Writing – Original Draft, K.Y.; Writing – Review & Editing, K.Y., S.N., A.S., Y.I., R.Y., P.S., K.Ta., T.I., C.Z., M.M., Y.O., S.N., H.K-H., M.O., S.A., Y.A., D.S., K.Ts., S.M., S.I., and Y.F.; Funding Acquisition, K.Y.; Supervision, M.O., K.Ts., S.M., S.I., and Y.F.

DECLARATION OF INTERESTS

The authors declare no competing interests.

INCLUSION AND DIVERSITY

We support inclusive, diverse, and equitable conduct of research.

REFERENCES

1. Fujisawa, T., and Filippakopoulos, P. (2017). Functions of bromodomain-containing proteins and their roles in homeostasis and cancer. Nat. Rev. Mol. Cell Biol. *18*, 246–262. https://doi.org/10.1038/nrm.2016.143.

2. French, C.A., Miyoshi, I., Kubonishi, I., Grier, H.E., Perez-Atayde, A.R., and Fletcher, J.A. (2003). BRD4-NUT fusion oncogene: a novel mechanism in aggressive carcinoma. Cancer Res. *63*, 304–307.

3. French, C.A., Ramirez, C.L., Kolmakova, J., Hickman, T.T., Cameron, M.J., Thyne, M.E., Kutok, J.L., Toretsky, J.A., Tadavarthy, A.K., Kees, U.R., et al. (2008). BRD-NUT oncoproteins: a family of closely related nuclear proteins that block epithelial differentiation and maintain the growth of carcinoma cells. Oncogene *27*, 2237–2242. https://doi.org/10.1038/sj.onc.1210852.

4. Baratta, M.G., Schinzel, A.C., Zwang, Y., Bandopadhayay, P., Bowman-Colin, C., Kutt, J., Curtis, J., Piao, H., Wong, L.C., Kung, A.L., et al. (2015). An in-tumor genetic screen reveals that the BET bromodomain protein, BRD4, is a potential therapeutic target in ovarian carcinoma. Proc. Natl. Acad. Sci. USA

112, 232–237. https://doi.org/10.1073/pnas. 1422165112.

5. Hnisz, D., Abraham, B.J., Lee, T.I., Lau, A., Saint-André, V., Sigova, A.A., Hoke, H.A., and Young, R.A. (2013). Super-enhancers in the control of cell identity and disease. Cell *155*, 934–947. https://doi.org/10.1016/j.cell.2013. 09.053.

6. Lovén, J., Hoke, H.A., Lin, C.Y., Lau, A., Orlando, D.A., Vakoc, C.R., Bradner, J.E., Lee, T.I., and Young, R.A. (2013). Selective inhibition of tumor oncogenes by disruption of super-enhancers. Cell *153*, 320–334. https://doi.org/10.1016/j.cell.2013.03.036.

7. Filippakopoulos, P., Qi, J., Picaud, S., Shen, Y., Smith, W.B., Fedorov, O., Morse, E.M., Keates, T., Hickman, T.T., Felletar, I., et al. (2010). Selective inhibition of BET bromodomains. Nature *468*, 1067–1073. https://doi.org/10.1038/nature09504.

8. Yamaguchi, K., Sakai, M., Shimokawa, T., Yamada, Y., Nakamura, Y., and Furukawa, Y. (2010). C20orf20 (MRG-binding protein) as a potential therapeutic target for colorectal cancer. Br. J. Cancer *102*, 325–331. https:// doi.org/10.1038/sj.bjc.6605500.

9. Yamaguchi, K., Sakai, M., Kim, J., Tsunesumi, S.i., Fujii, T., Ikenoue, T., Yamada, Y., Akiyama, Y., Muto, Y., Yamaguchi, R., et al. (2011). MRG-binding protein contributes to colorectal cancer development. Cancer Sci. *102*, 1486–1492. https://doi.org/10.1111/j. 1349-7006.2011.01971.x.

10. Scotto, L., Narayan, G., Nandula, S.V., Arias-Pulido, H., Subramaniyam, S., Schneider, A., Kaufmann, A.M., Wright, J.D., Pothuri, B., Mansukhani, M., and Murty, V.V. (2008). Identification of copy number gain and overexpressed genes on chromosome arm 20q by an integrative genomic approach in cervical cancer: potential role in progression. Genes Chromosomes Cancer *47*, 755–765. https://doi.org/10.1002/gcc.20577.

11. Watt, S.A., Pourreyron, C., Purdie, K., Hogan, C., Cole, C.L., Foster, N., Pratt, N., Bourdon, J.C., Appleyard, V., Murray, K., et al. (2011). Integrative mRNA profiling comparing cultured primary cells with clinical samples reveals PLK1 and C20orf20 as therapeutic targets in cutaneous squamous cell carcinoma. Oncogene *30*, 4666–4677. https:// doi.org/10.1038/onc.2011.180.

12. Ding, F., Zhang, S., Gao, S., Shang, J., Li, Y., Cui, N., and Zhao, Q. (2017). MRGBP as a potential biomarker for the malignancy of pancreatic ductal adenocarcinoma. Oncotarget *8*, 64224–64236. https://doi.org/ 10.18632/oncotarget.19451.

13. Doyon, Y., and Côté, J. (2004). The highly conserved and multifunctional NuA4 HAT complex. Curr. Opin. Genet. Dev. *14*, 147–154. https://doi.org/10.1016/j.gde.2004. 02.009.

14. Doyon, Y., Selleck, W., Lane, W.S., Tan, S., and Côté, J. (2004). Structural and functional conservation of the NuA4 histone acetyltransferase complex from yeast to humans. Mol. Cell Biol. *24*, 1884–1896.

15. Jacquet, K., Fradet-Turcotte, A., Avvakumov, N., Lambert, J.P., Roques, C., Pandita, R.K., Paquet, E., Herst, P., Gingras, A.C., Pandita, T.K., et al. (2016). The TIP60 complex regulates bivalent chromatin recognition by 53BP1 through direct H4K20me binding and H2AK15 acetylation. Mol. Cell *62*, 409–421. https://doi.org/10.1016/j.molcel.2016. 03.031.

16. Gorrini, C., Squatrito, M., Luise, C., Syed, N., Perna, D., Wark, L., Martinato, F., Sardella, D., Verrecchia, A., Bennett, S., et al. (2007). Tip60 is a haplo-insufficient tumour suppressor required for an oncogene-induced DNA damage response. Nature *448*, 1063–1067. https://doi.org/10.1038/nature06055.

17. Tang, Y., Luo, J., Zhang, W., and Gu, W. (2006). Tip60-dependent acetylation of p53 modulates the decision between cell-cycle arrest and apoptosis. Mol. Cell *24*, 827–839. https://doi.org/10.1016/j.molcel.2006. 11.021.

18. Yamada, H.Y., and Rao, C.V. (2009). BRD8 is a potential chemosensitizing target for spindle poisons in colorectal cancer therapy. Int. J. Oncol. *35*, 1101–1109. https://doi.org/10. 3892/ijo_00000425.

19. Lashgari, A., Fauteux, M., Maréchal, A., and Gaudreau, L. (2018). Cellular depletion of BRD8 causes p53-dependent apoptosis and induces a DNA damage response in non-stressed cells. Sci. Rep. *8*, 14089. https://doi. org/10.1038/s41598-018-32323-3.

20. Yu, Z., Chen, T., Mo, H., Guo, C., and Liu, Q. (2020). BRD8, which is negatively regulated by miR-876-3p, promotes the proliferation and apoptosis resistance of hepatocellular carcinoma cells via KAT5. Arch. Biochem. Biophys. *693*, 108550. https://doi.org/10. 1016/j.abb.2020.108550.

21. Tamkun, J.W., Deuring, R., Scott, M.P., Kissinger, M., Pattatucci, A.M., Kaufman, T.C., and Kennison, J.A. (1992). brahma: a regulator of Drosophila homeotic genes structurally related to the yeast transcriptional activator SNF2/SWI2. Cell *68*, 561–572. https://doi.org/10.1016/0092-8674(92)90191-e.

22. Dhalluin, C., Carlson, J.E., Zeng, L., He, C., Aggarwal, A.K., and Zhou, M.M. (1999). Structure and ligand of a histone acetyltransferase bromodomain. Nature *399*, 491–496. https://doi.org/10.1038/20974.

23. Allard, S., Utley, R.T., Savard, J., Clarke, A., Grant, P., Brandl, C.J., Pillus, L., Workman, J.L., and Côté, J. (1999). NuA4, an essential transcription adaptor/histone H4 acetyltransferase complex containing Esa1p and the ATM-related cofactor Tra1p. EMBO J. *18*, 5108–5119. https://doi.org/10.1093/ emboj/18.18.5108.

24. Ikura, T., Ogryzko, V.V., Grigoriev, M., Groisman, R., Wang, J., Horikoshi, M., Scully, R., Qin, J., and Nakatani, Y. (2000). Involvement of the TIP60 histone acetylase complex in DNA repair and apoptosis. Cell

102, 463–473. https://doi.org/10.1016/s0092-8674(00)00051-9.

25. Robers, M.B., Dart, M.L., Woodroofe, C.C., Zimprich, C.A., Kirkland, T.A., Machleidt, T., Kupcho, K.R., Levin, S., Hartnett, J.R., Zimmerman, K., et al. (2015). Target engagement and drug residence time can be observed in living cells with BRET. Nat. Commun. *6*, 10091. https://doi.org/10.1038/ ncomms10091.

26. Hayakawa, T., Ohtani, Y., Hayakawa, N., Shinmyozu, K., Saito, M., Ishikawa, F., and Nakayama, J.i. (2007). RBP2 is an MRG15 complex component and down-regulates intragenic histone H3 lysine 4 methylation. Gene Cell. *12*, 811–826. https://doi.org/10. 1111/j.1365-2443.2007.01089.x.

27. Tsherniak, A., Vazquez, F., Montgomery, P.G., Weir, B.A., Kryukov, G., Cowley, G.S., Gill, S., Harrington, W.F., Pantel, S., Krill-Burger, J.M., et al. (2017). Defining a cancer dependency Map. Cell *170*, 564–576.e16. https://doi.org/ 10.1016/j.cell.2017.06.010.

28. Niida, A., Smith, A.D., Imoto, S., Aburatani, H., Zhang, M.Q., and Akiyama, T. (2009). Gene set-based module discovery in the breast cancer transcriptome. BMC Bioinformatics *10*, 71. https://doi.org/10. 1186/1471-2105-10-71.

29. Chevillard-Briet, M., Quaranta, M., Grézy, A., Mattera, L., Courilleau, C., Philippe, M., Mercier, P., Corpet, D., Lough, J., Ueda, T., et al. (2014). Interplay between chromatin-modifying enzymes controls colon cancer progression through Wnt signaling. Hum. Mol. Genet. *23*, 2120–2131. https://doi.org/ 10.1093/hmg/ddt604.

30. Brady, M.E., Ozanne, D.M., Gaughan, L., Waite, I., Cook, S., Neal, D.E., and Robson, C.N. (1999). Tip60 is a nuclear hormone receptor coactivator. J. Biol. Chem. *274*, 17599–17604. https://doi.org/10.1074/jbc. 274.25.17599.

31. Hosoya, T., Monden, T., Fukabori, Y., Hashimoto, K., Satoh, T., Kasai, K., Yamada, M., and Mori, M. (2008). A novel splice variant of the nuclear coactivator p120 functions strongly for androgen receptor: characteristic expression in prostate disease. Endocr. J. *55*, 657–665. https://doi.org/10.1507/endocrj. k07e-133.

32. Monden, T., Kishi, M., Hosoya, T., Satoh, T., Wondisford, F.E., Hollenberg, A.N., Yamada, M., and Mori, M. (1999). p120 acts as a specific coactivator for 9-cis-retinoic acid receptor (RXR) on peroxisome proliferator-activated receptor-gamma/RXR heterodimers. Mol. Endocrinol. *13*, 1695–1703. https://doi.org/ 10.1210/mend.13.10.0353.

33. Monden, T., Wondisford, F.E., and Hollenberg, A.N. (1997). Isolation and characterization of a novel ligand-dependent thyroid hormone receptor-coactivating protein. J. Biol. Chem. *272*, 29834–29841. https://doi.org/10.1074/jbc.272.47.29834.

34. Wu, S.Y., Lee, C.F., Lai, H.T., Yu, C.T., Lee, J.E., Zuo, H., Tsai, S.Y., Tsai, M.J., Ge, K., Wan, Y., and Chiang, C.M. (2020). Opposing functions of BRD4 isoforms in breast cancer.

Mol. Cell 78, 1114–1132.e10. https://doi.org/10.1016/j.molcel.2020.04.034.

35. Jiang, C.Y., Ruan, Y., Wang, X.H., Zhao, W., Jiang, Q., Jing, Y.F., Han, B.M., Xia, S.J., and Zhao, F.J. (2016). MiR-185 attenuates androgen receptor function in prostate cancer indirectly by targeting bromodomain containing 8 isoform 2, an androgen receptor co-activator. Mol. Cell. Endocrinol. 427, 13–20. https://doi.org/10.1016/j.mce.2016.02.023.

36. Bunz, F., Dutriaux, A., Lengauer, C., Waldman, T., Zhou, S., Brown, J.P., Sedivy, J.M., Kinzler, K.W., and Vogelstein, B. (1998). Requirement for p53 and p21 to sustain G2 arrest after DNA damage. Science 282, 1497–1501. https://doi.org/10.1126/science.282.5393.1497.

37. Leone, G., DeGregori, J., Yan, Z., Jakoi, L., Ishida, S., Williams, R.S., and Nevins, J.R. (1998). E2F3 activity is regulated during the cell cycle and is required for the induction of S phase. Genes Dev. 12, 2120–2130. https://doi.org/10.1101/gad.12.14.2120.

38. Ishimi, Y. (2018). Regulation of MCM2-7 function. Genes Genet. Syst. 93, 125–133. https://doi.org/10.1266/ggs.18-00026.

39. Ibarra, A., Schwob, E., and Méndez, J. (2008). Excess MCM proteins protect human cells from replicative stress by licensing backup origins of replication. Proc. Natl. Acad. Sci. USA 105, 8956–8961. https://doi.org/10.1073/pnas.0803978105.

40. Lau, E., Tsuji, T., Guo, L., Lu, S.H., and Jiang, W. (2007). The role of pre-replicative complex (pre-RC) components in oncogenesis. FASEB J. 21, 3786–3794. https://doi.org/10.1096/fj.07-8900rev.

41. Tsao, C.C., Geisen, C., and Abraham, R.T. (2004). Interaction between human MCM7 and Rad17 proteins is required for replication checkpoint signaling. EMBO J. 23, 4660–4669. https://doi.org/10.1038/sj.emboj.7600463.

42. Snyder, M., He, W., and Zhang, J.J. (2005). The DNA replication factor MCM5 is essential for Stat1-mediated transcriptional activation. Proc. Natl. Acad. Sci. USA 102, 14539–14544. https://doi.org/10.1073/pnas.0507479102.

43. Sedlackova, H., Rask, M.B., Gupta, R., Choudhary, C., Somyajit, K., and Lukas, J. (2020). Equilibrium between nascent and parental MCM proteins protects replicating genomes. Nature 587, 297–302. https://doi.org/10.1038/s41586-020-2842-3.

44. Drissi, R., Chauvin, A., McKenna, A., Lévesque, D., Blais-Brochu, S., Jean, D., and Boisvert, F.M. (2018). Destabilization of the MiniChromosome Maintenance (MCM) complex modulates the cellular response to DNA double strand breaks. Cell Cycle 17, 2593–2609. https://doi.org/10.1080/15384101.2018.1553336.

45. Inoue, D., Chew, G.L., Liu, B., Michel, B.C., Pangallo, J., D'Avino, A.R., Hitchman, T., North, K., Lee, S.C.W., Bitner, L., et al. (2019). Spliceosomal disruption of the non-canonical BAF complex in cancer. Nature 574, 432–436. https://doi.org/10.1038/s41586-019-1646-9.

46. Remillard, D., Savage, N.A., Kedves, A.T., Paulk, J., Chen, X., Garcia, F.J., Romanowski, M.J., Horton, P.A., Murphy, J., Schirle, M., et al. (2021). Chemoproteomics enabled discovery of selective probes for NuA4 factor BRD8. ACS Chem. Biol. 16, 2185–2192. https://doi.org/10.1021/acschembio.1c00256.

47. Browne, J.A., NandyMazumdar, M., Paranjapye, A., Leir, S.H., and Harris, A. (2021). The Bromodomain Containing 8 (BRD8) transcriptional network in human lung epithelial cells. Mol. Cell. Endocrinol. 524, 111169. https://doi.org/10.1016/j.mce.2021.111169.

48. Behrens, J., Jerchow, B.A., Würtele, M., Grimm, J., Asbrand, C., Wirtz, R., Kühl, M., Wedlich, D., and Birchmeier, W. (1998). Functional interaction of an axin homolog, conductin, with beta-catenin, APC, and GSK3beta. Science 280, 596–599. https://doi.org/10.1126/science.280.5363.596.

49. Leung, J.Y., Kolligs, F.T., Wu, R., Zhai, Y., Kuick, R., Hanash, S., Cho, K.R., and Fearon, E.R. (2002). Activation of AXIN2 expression by beta-catenin-T cell factor. A feedback repressor pathway regulating Wnt signaling. J. Biol. Chem. 277, 21657–21665. https://doi.org/10.1074/jbc.M200139200.

50. Yamaguchi, K., Nagatoishi, S., Tsumoto, K., and Furukawa, Y. (2020). Discovery of chemical probes that suppress Wnt/beta-catenin signaling through high-throughput screening. Cancer Sci. 111, 783–794. https://doi.org/10.1111/cas.14297.

51. Dobin, A., Davis, C.A., Schlesinger, F., Drenkow, J., Zaleski, C., Jha, S., Batut, P., Chaisson, M., and Gingeras, T.R. (2013). STAR: ultrafast universal RNA-seq aligner. Bioinformatics 29, 15–21. https://doi.org/10.1093/bioinformatics/bts635.

52. Li, B., and Dewey, C.N. (2011). RSEM: accurate transcript quantification from RNA-Seq data with or without a reference genome. BMC Bioinformatics 12, 323. https://doi.org/10.1186/1471-2105-12-323.

53. Love, M.I., Huber, W., and Anders, S. (2014). Moderated estimation of fold change and dispersion for RNA-seq data with DESeq2. Genome Biol. 15, 550. https://doi.org/10.1186/s13059-014-0550-8.

54. Langmead, B., and Salzberg, S.L. (2012). Fast gapped-read alignment with Bowtie 2. Nat. Methods 9, 357–359. https://doi.org/10.1038/nmeth.1923.

55. Zhang, Y., Liu, T., Meyer, C.A., Eeckhoute, J., Johnson, D.S., Bernstein, B.E., Nusbaum, C., Myers, R.M., Brown, M., Li, W., and Liu, X.S. (2008). Model-based analysis of ChIP-seq (MACS). Genome Biol. 9, R137. https://doi.org/10.1186/gb-2008-9-9-r137.

56. Heinz, S., Benner, C., Spann, N., Bertolino, E., Lin, Y.C., Laslo, P., Cheng, J.X., Murre, C., Singh, H., and Glass, C.K. (2010). Simple combinations of lineage-determining transcription factors prime cis-regulatory elements required for macrophage and B cell identities. Mol. Cell 38, 576–589. https://doi.org/10.1016/j.molcel.2010.05.004.

57. Yamaguchi, K., Yamaguchi, R., Takahashi, N., Ikenoue, T., Fujii, T., Shinozaki, M., Tsurita, G., Hata, K., Niida, A., Imoto, S., et al. (2014). Overexpression of cohesion establishment factor DSCC1 through E2F in colorectal cancer. PLoS One 9, e85750. https://doi.org/10.1371/journal.pone.0085750.

STAR★METHODS

KEY RESOURCES TABLE

REAGENT or RESOURCE	SOURCE	IDENTIFIER
Antibodies		
Rabbit polyclonal anti-BRD8	Sigma-Aldrich	Cat# HPA001841; RRID:AB_1845438
Rabbit polyclonal anti-BRD8	Active Motif	Cat# 61008; RRID:AB_2615053
Rabbit polyclonal anti-BRD8	Bethyl	Cat# IHC-00020; RRID:AB_2066033
Rabbit polyclonal anti-BRD8	Santa Cruz Biotechnology	Cat# sc-130108; RRID:AB_2066032
Rabbit polyclonal anti-TIP60	Millipore	Cat# DR1041; RRID:AB_2128436
Rabbit polyclonal anti-C20orf20 (MRGBP)	Sigma-Aldrich	Cat# HPA017012; RRID:AB_1845679
Rat monoclonal anti-ORC2	Santa Cruz Biotechnology	Cat# sc-32734; RRID:AB_2157726
Mouse monoclonal anti-MCM3	Santa Cruz Biotechnology	Cat# sc-390480; RRID:N/A
Mouse monoclonal anti-MCM6	Santa Cruz Biotechnology	Cat# sc-393618; RRID:AB_2885187
Mouse monoclonal anti-MCM7	Santa Cruz Biotechnology	Cat# sc-9966; RRID:AB_627235
Rabbit polyclonal anti-MCMBP	Atlas Antibodies	Cat# HPA038481; RRID:AB_10794620
Mouse monoclonal anti-p53	Santa Cruz Biotechnology	Cat# sc-126; RRID:AB_628082
Rabbit monoclonal anti-c-Fos	Cell Signaling Technology	Cat# 2250; RRID:AB_2247211
Rabbit monoclonal anti-FRA1	Cell Signaling Technology	Cat# 5281; RRID:AB_10557418
Rabbit monoclonal anti-Fra2	Cell Signaling Technology	Cat# 19967; RRID:AB_2722526
Rabbit monoclonal anti-Axin2	Cell Signaling Technology	Cat# 2151; RRID:AB_2062432
Rabbit monoclonal anti-Phospho-Histone H2A.X (Ser139)	Cell Signaling Technology	Cat# 9718; RRID:AB_2118009
Rabbit monoclonal anti-Phospho-RPA32/RPA2 (Ser8)	Cell Signaling Technology	Cat# 54762; RRID:AB_2799471
Mouse monoclonal anti-β-Actin	Sigma-Aldrich	Cat# A5441; RRID:AB_476744
Goat polyclonal anti-Lamin B	Santa Cruz Biotechnology	Cat# sc-6216; RRID:AB_648156
Mouse monoclonal anti-β-Tublin	Sigma-Aldrich	Cat# T4026; RRID:AB_477577
Rat monoclonal anti-HA (3F10)	Roche	Cat# 11867431001; RRID:AB_390919
Rabbit polyclonal anti-HA	Abcam	Cat# ab9110; RRID:AB_307019
Mouse monoclonal anti-FLAG (M2)	Sigma-Aldrich	Cat# F4049; RRID:AB_439701
Mouse monoclonal anti-c-Myc (9E10)	Sigma-Aldrich	Cat# M5546; RRID:AB_260581
Anti-mouse IgG, HRP-linked whole Ab sheep	Cytiva	Cat# NA931; RRID:N/A
Anti-rat IgG, HRP-linked whole Ab goat	Cytiva	Cat# NA935; RRID:N/A
Anti-rabbit IgG, HRP-linked F(ab')2 fragment donkey	Cytiva	Cat# NA9340; RRID:N/A
F(ab')2-goat anti-rabbit IgG (H+L) secondary antibody, Alexa Fluor 568	Thermo Fisher Scientific	Cat# A-21069; RRID:AB_2535730
Chemicals, peptides, and recombinant proteins		
Propidium iodide	Sigma-Aldrich	Cat# P4170
RNase A	Sigma-Aldrich	Cat# R6513
Cycloheximide	Fujifilm Wako Pure Chemical	Cat# 037-20991
Puromycin	Sigma-Aldrich	Cat# P8833
MG132	Merck	Cat# 474790
Proteinase K	Merck	Cat# P2308
JQ1	Cayman	Cat# 11187
Mounting Medium with DAPI	Vector Laboratories	Cat# H-1200

(Continued on next page)

Continued

REAGENT or RESOURCE	SOURCE	IDENTIFIER
Critical commercial assays		
KAPA SYBR Fast qPCR kit	Kapa Biosystems	Cat# KK4602
Cell Cycle Assay Solution Blue	Dojindo	Cat# C549
Cell Counting Kit-8	Dojindo	Cat# CK04
Click-iT Plus EdU Alexa Fluor 488 Flow Cytometry Assay Kit	Thermo Fisher Scientific	Cat# C10632
CellTiter-Glo 3D Cell Viability Assay	Promega	Cat# G9681
Nuclear Extract Kit	Active Motif	Cat# 40010
NanoBRET Nano-Glo Detection Systems	Promega	Cat# N1661
PTMScan HS Ubiquitin/SUMO Remnant Motif (K-ε-GG) Kit	Cell Signaling Technology	Cat# 59322
NEBNext Ultra II Directional RNA Library Prep Kit	New England Biolabs	Cat# E7760
NEBNext Ultra II DNA Library Prep kit	New England Biolabs	Cat# E7645
Deposited data		
RNA-seq data	This paper	GEO: GSE203236
BRD8 ChIP-seq data	This paper	GEO: GSE203615
TIP60 ChIP-seq data	Jacquet et al.[15]	GEO: GSE78027
Multi-tissue RNA-seq data	The Genotype-Tissue Expression (GTEx)	https://gtexportal.org/home/
TCGA-COAD data	The Cancer Genome Atlas (TCGA)	https://portal.gdc.cancer.gov/
Experimental models: Cell lines		
HCT116	ATCC	cat# CCL-247; RRID:CVCL_0291
SW480	ATCC	cat# CCL-228; RRID:CVCL_0546
HT-29	ATCC	cat# HTB-38; RRID:CVCL_0320
HCT-15	ATCC	cat# CCL-225; RRID:CVCL_0292
DLD-1	ATCC	cat# CCL-221; RRID:CVCL_0248
LoVo	ATCC	cat# CCL-229; RRID:CVCL_0399
LS174T	ATCC	ATCC cat# CL-188; RRID:CVCL_1384
SW48	ATCC	cat# CCL-231; RRID:CVCL_1724
SW948	ATCC	cat# CCL-237; RRID:CVCL_0632
COS-7	ATCC	cat# CRL-1651; RRID:CVCL_0224
HCT116 p53$^{-/-}$	Dr. Bert Vogelstein (Johns Hopkins University)[36]	N/A
293FT	Thermo Fisher Scientific	cat# R70007; RRID:CVCL_6911
Experimental models: Organisms/strains		
BALB/cAJcl-*nu/nu*	CLEA Japan	N/A
Oligonucleotides		
Primers for qPCR, cloning, and mutagenesis, see Table S8	This paper	N/A
siRNA and gRNA target sequences, see Table S8	This paper	N/A

Continued

REAGENT or RESOURCE	SOURCE	IDENTIFIER
Recombinant DNA		
pCAGGS-HA BRD8 (wt and mutants)	This paper	N/A
pcDNA3.1-Myc/His MRGBP	Yamaguchi et al.[8]	N/A
pCAGGS-3×Flag MRGBP	This paper	N/A
pCAGGS-HA TIP60, MRG15, MRGX, EPC1, ING3	This paper	N/A
pcDNA4-TO-HA-Brd4FL	Addgene	Cat# 31351
pNLF1-N BRD8 (wt and mutant), BRD4 (wt and mutant)	This paper	N/A
pHTC Halo Tag histone H4	This paper	N/A
pMXs-Puro vector	Dr. Toshio Kitamura (The University of Tokyo)	N/A
pME-FLAG/His-Ub	Dr. Chihiro Sasakawa (The University of Tokyo)	N/A
Software and algorithms		
FlowJo software	Becton Dickinson	N/A
SEQUEST HT algorithm in Proteome Discoverer Software (v2.5)	Thermo Fisher Scientific	N/A
STAR (v2.7.3a)	Dobin et al.[51]	https://github.com/alexdobin/STAR
RSEM (v1.3.3)	Li et al.[52]	https://github.com/deweylab/RSEM
DESeq2 package (v1.26.0)	Love et al.[53]	https://github.com/mikelove/DESeq2
Investigate Human Gene Sets in GSEA	Broad Institute	http://www.gsea-msigdb.org/gsea/msigdb/human/annotate.jsp
EEM2.0	Niida et al.[28]	https://github.com/atusiniida/EEM2.0
Bowtie2 (v2.4.1)	Langmead et al.[54]	https://github.com/BenLangmead/bowtie2
MACS2 (v3.6)	Zhang et al.[55]	https://github.com/macs3-project/MACS
HOMER (v4.11)	Heinz et al.[56]	http://homer.ucsd.edu/homer/introduction/install.html

RESOURCE AVAILABILITY

Lead contact
Further information and requests for resources and reagents should be directed to and will be fulfilled by the lead contact: Kiyoshi Yamaguchi (kiyamagu@g.ecc.u-tokyo.ac.jp).

Materials availability
This study did not generate new animal models and reagents.

Data and code availability
- Data: All data generated or analyzed during this study are included in this article and its supplemental information files. RNA-seq (GSE203236) and ChIP-seq (GSE203615) data were deposited in the Gene Expression Omnibus (GEO) database. Multi-tissue RNA-seq data were downloaded from the GTEx project (dbGaP accession number phs000424.v8.p2). TIP60 ChIP-seq data were downloaded from GEO (GSE78027).

- Code: This paper does not report original code.

- All other requests: Any additional information required to reanalyze the data reported in this paper is available from the lead contact upon request.

EXPERIMENTAL MODEL AND SUBJECT DETAILS

Cell lines and culture conditions

Human colorectal cancer cells and African green monkey kidney cells were obtained from the American Type Culture Collection (Manassas, VA, USA). HCT116 p53-/- cells were kindly provided by Dr. Bert Vogelstein (Johns Hopkins University).[36] These cells were maintained in appropriate media (Dulbecco's Modified Eagle Medium for COS-7 and HCT116 p53-/-; McCoy's 5A Modified Medium for HCT116; Leibovitz's L-15 Medium for SW480, SW48, and SW948; Minimum Essential Media for LS174T; Ham's F-12 Nutrient Mix for LoVo; and RPMI 1640 Media for HT-29, HCT-15, and DLD-1) supplemented with 10% fetal bovine serum (Biosera, Nuaille, France) and 1% penicillin/streptomycin solution (Fujifilm Wako Pure Chemical, Osaka, Japan). 293FT cells derived from human embryonal kidney cells transformed with the SV40 large T antigen were obtained from Thermo Fisher Scientific (Waltham, MA, USA). The cells were maintained in Dulbecco's Modified Eagle Medium supplemented with 10% fetal bovine serum, 1% penicillin/streptomycin solution, 0.1 mM MEM Non-Essential Amino Acids Solution (Thermo Fisher Scientific), 6 mM L-glutamine (Thermo Fisher Scientific), 1 mM Sodium Pyruvate (Thermo Fisher Scientific), and 500 µg/ml Geneticin Selective Antibiotic (Thermo Fisher Scientific). Clinical data for each patient are summarized in Table S9.

Colorectal tumor tissues

This study was approved by the institutional review board of the Institute of Medical Science, the University of Tokyo (IMSUT-IRB, 2020-78-0318). Colorectal tumor tissues and corresponding non-cancerous tissues were obtained with written informed consent from patients who underwent surgery in the Research Hospital of IMSUT.

Xenograft tumor in nude mice

Animal experiments were conducted in accordance with the institutional ethical guidelines for animal experiments. Experimental protocols were approved by the Animal Care and Use Committee of the Institute of Medical Science, the University of Tokyo. Six-week-old male BALB/c nude mice were purchased from Clea Japan (Tokyo, Japan). BRD8-KO and parental HCT116 (8×10^5) or SW948 cells (1.5×10^6) in 0.2 mL PBS were subcutaneously injected into the nude mice (n = 6–7). Tumor tissues from sacrificed mice were removed at 20th (HCT116) and 27th (SW948) day post inoculation, and the tumor mass was weighed by a balance.

METHOD DETAILS

Gene silencing

Synthetic siRNA oligos targeting *BRD8* and *TIP60* were obtained from Merck (Darmstadt, Germany), and those targeting *ORC2*, *MCM3*, *MCM6*, *MCM7*, *FOS*, *FOSL1*, *FOSL2*, *JUN*, and *JUNB* were obtained from Integrated DNA Technologies (Coralville, IA, USA). A negative control siRNA (ON-TARGETplus Non-targeting Control) was obtained from Horizon Discovery (Cambridge, UK). The target sequences of siRNAs are shown in Table S8. Cells were transfected with 10 nM of siRNA using Lipofectamine RNAiMAX (Thermo Fisher Scientific), and were harvested after 48 h of incubation.

Plasmids

pCAGGS-HA BRD8 (isoform 1: GenBank: NM_006696.4, isoform 2: GenBank: NM_139199.2) and pcDNA3.1-Myc/His MRGBP (GenBank: NM_018270.6) were constructed as described previously.[8] pcDNA4-TO-HA-Brd4FL was obtained from Addgene (#31351, Cambridge, MA, USA). The entire coding regions of *MRG15* (GenBank: NM_006791.4), *MRGX* (GenBank: NM_012286.3), *TIP60* (GenBank: NM_182710.3), *EPC1* (GenBank: NM_001272004.3), and *ING3* (GenBank: NM_019071.3) cDNAs were amplified by RT-PCR using a set of primers (Table S8) and RNA obtained from healthy volunteers. The PCR products were cloned into an appropriate cloning site of pCAGGS-HA vector. Coding region of *MRGBP* was amplified by PCR using pcDNA3.1-Myc/His MRGBP as a template, and subcloned into the *Eco*RI and *Xho*I cloning sites of pCMV-Myc-N vector (Takara Bio, Shiga, Japan) and pCAGGS-3×Flag vector. To generate plasmid expressing deletion mutant of MRGBP (Δ24–90), codons 1–23 and 91–204 of *MRGBP* cDNA were separately amplified and subcloned into pCMV-Myc-N vector. To generate plasmids containing deletion mutants of BRD8, different regions of *BRD8* were amplified by PCR using pCAGGS-HA BRD8 as a template. The PCR products were subcloned into an appropriate cloning site of pCAGGS-HA vector. The primer sequences used for the amplification are shown in Table S8. DNA sequences of all

constructs were confirmed by DNA sequencing (3730 DNA Analyzer or 3500xL Genetic Analyzer, Thermo Fisher Scientific).

Quantitative PCR (qPCR)

A SYBR green-based qPCR was performed on StepOnePlus or QuantStudio 3 systems (Thermo Fisher Scientific) using KAPA SYBR Fast qPCR kit (Kapa Biosystems, Wilmington, MA, USA). Amounts of transcripts were determined by relative standard curve method, and glyceraldehyde-3-phosphate dehydrogenase (*GAPDH*) was used as an internal control. Sequences of primers used for the qPCR are listed in Table S8.

Construction of RNAi-resistant plasmids and rescue experiment

Silent mutations within the coding sequence of BRD8 were introduced by site-directed mutagenesis. pCAGGS-HA BRD8 (WT) or pCAGGS-HA BRD8 (ΔB) with the desired mutations were amplified using KOD-Plus-Neo (Toyobo, Osaka, Japan) and a set of primers as listed in Table S8. The PCR products were digested with *Dpn* I (Takara Bio) for 2 h at 37°C, followed by transformation into *E. coli*. Incorporation of mutations within the plasmids was confirmed by Sanger sequencing.

The RNAi-resistant BRD8-FL (rBRD8-FL) and BRD8-ΔB (rBRD8-ΔB) were subcloned into the retroviral vector pMX. The pMX vector, pMX EGFP, and a Plat-A packaging cell line were kindly provided by Dr. Toshio Kitamura (The University of Tokyo). The Plat-A cells were transfected with pMX EGFP, pMX rBRD8-FL, or pMX rBRD8-ΔB using FuGENE6 (Promega, Madison, WI, USA). The virus supernatants were added into the culture media of HCT116 cells. 48 h after infection, the cells were selected with media containing puromycin (0.4 μg/ml) for 5 days.

Flow cytometry

Cultured cells were transfected with the indicated siRNAs for 48 h using Lipofectamine RNAiMAX (Thermo Fisher Scientific). After washing with PBS, unfixed cells were treated with Cell Cycle Assay Solution Blue (Dojindo, Kumamoto, Japan) at 37°C for 15 min. To stain the cells with propidium iodide (PI), they were fixed with 70% ethanol, and kept at −20°C before use. The cells were then incubated with 2 mg/ml RNase A at 37°C for 30 min and stained with PI at room temperature for 30 min. Subsequently, the cell suspensions were analyzed on the BD FACSCanto II system (Becton Dickinson, Franklin Lakes, NJ, USA). Data analysis was performed using FlowJo software (Becton Dickinson).

Cell viability assay

siRNAs were introduced into CRC cells in 96-well plates by reverse transfection method using Lipofectamine RNAiMAX (Thermo Fisher Scientific). Four days after transfection, viable cells were measured using Cell Counting Kit-8 (Dojindo), a water-soluble tetrazolium salt (WST)-based assay. In the case of 3D culture, siRNAs were also introduced into the cells in 96-wells plates with round bottom ultra-low attachment (PrimeSurface, Sumitomo Bakelite, Tokyo, Japan). Four days after transfection, the number of viable cells was measured based on the amount of ATP present (CellTiter-Glo 3D Cell Viability Assay, Promega).

Immunocytochemical staining

COS-7 cells were transfected with pCAGGS-HA BRD8 (FL) or pCAGGS-HA BRD8 (ΔN) using FuGENE6 (Promega). Twenty-four hours after transfection, the cells fixed with paraformaldehyde were rendered permeable with PBS containing 0.1% Triton X-100. The cells were covered with 3% bovine serum albumin in PBS to block non-specific hybridization, and subsequently incubated with anti-HA antibody (Abcam, Cambridge, UK, Cat# ab9110, RRID:AB_307019). The reaction was visualized after incubation with Alexa Fluor 568 anti-rabbit secondary antibody (Thermo Fisher Scientific). Nuclei were counterstained with 4′,6-diamidino-2-phenylindole, dihydrochloride (DAPI, Vector Laboratories, Burlingame, CA, USA). The images were captured by a confocal laser microscope (Nikon A1, Nikon, Tokyo, Japan).

Cycloheximide chase assay

HEK293FT cells were transfected with pCAGGS-HA BRD8 (WT) or pCAGGS-HA BRD8 (ΔB) in combination with pCAGGS-3×Flag MRGBP using ViaFect (Promega). Twenty-four hours after transfection, the cell culture medium was changed to the medium containing 100 μg/ml cycloheximide (Fujifilm Wako Pure Chemical). The cells were harvested at the indicated time points and the cell lysates were analyzed by immunoblotting.

Immunoblot analysis

Cells were lysed in radioimmunoprecipitation assay buffer (50 mM Tris-HCl, pH 8.0, 150 mM NaCl, 0.5% sodium deoxycholate, 1% Nonidet P-40, 0.1% sodium dodecyl sulphate) supplemented with a Protease Inhibitor Cocktail Set III (Merck). Proteins were separated by SDS-PAGE and immunoblot analysis was performed as described elsewhere.[8] Horseradish peroxidase-conjugated sheep anti-mouse (NA931V, Cytiva, Marlborough, MA, USA), goat anti-rat (NA935V, Cytiva), and donkey anti-rabbit IgG (NA9340V, Cytiva) served as the secondary antibody for chemiluminescent detection. ImmunoStar LD (Fujifilm Wako Pure Chemical) was used as chemiluminescence reagent and images were taken with the Amersham Imager 600 (Cytiva).

Immunoprecipitation

HEK293FT cells were transfected with pCAGGS-HA BRD8 (WT), pCAGGS-HA BRD8 (ΔC), or pCAGGS-HA BRD8 (ΔB) using FuGENE6 (Promega). Forty-eight hours after transfection, the cells were lysed in 0.4% Nonidet P-40 buffer (10 mM Tris-HCl pH7.5, 150 mM NaCl) supplemented with a Protease Inhibitor Cocktail Set (Merck). Pre-cleared cell extracts were incubated with anti-HA (Roche Cat# 11867431001, RRID:AB_390919) or anti-Myc antibody (Sigma-Aldrich Cat# M5546, RRID:AB_260581), followed by the incubation with Protein G-Sepharose beads (Cytiva) at 4°C. The immunocomplexes were then washed with 0.4% Nonidet P-40 buffer and subjected to immunoblotting. To evaluate the interactions between BRD8 and the FOS family members, nuclear fraction (Nuclear Extract Kit, Active Motif, Carlsbad, CA, USA) isolated from HCT116 or SW480 cells was subjected to immunoprecipitation with anti-c-Fos (Cell Signaling Technology, Danvers, MA, USA, Cat# 2250, RRID:AB_2247211), FRA1 (Cell Signaling Technology Cat# 5281, RRID:AB_10557418), or Fra2 (Cell Signaling Technology Cat# 19967, RRID:AB_2722526) antibody, followed by immunoblotting with anti-BRD8 (Sigma-Aldrich Cat# HPA001841, RRID:AB_1845438) or anti-TIP60 antibody (Millipore Cat# DR1041, RRID:AB_2128436).

Nuclear extraction

HEK293FT cells were transfected with pcDNA-Myc/His MRGBP in combination with pCAGGS-HA BRD8 (WT), pCAGGS-HA BRD8 (ΔN), or pCAGGS-HA BRD8 (ΔNB). Twenty-four hours after transfection, the cells were divided into cytoplasm and nuclear fractions using Nuclear Extract Kit (Active Motif). The lysates were subjected to immunoblotting.

Cell-based ubiquitination assay

HEK293FT cells were transfected with HA-BRD8 (pCAGGS-HA BRD8-WT) and pME-FLAG/His-Ub (kindly provided by Dr. Chihiro Sasakawa, The University of Tokyo) in combination with or without Myc-MRGBP (pCMV-Myc MRGBP-WT or -Δ24-90) using FuGENE6 (Promega). 36 h after transfection, the cells were treated with MG132 (8 μM) overnight, and then lysed in buffer A (6 M guanidine hydrochloride and 10 mM imidazole in Tris-buffered saline). The lysates were passed 10 times through a 23 G needle, followed by 20 times through a 26 G needle. Ubiquitinated proteins in the lysates were captured by incubating with Ni-NTA Agarose beads (Fujifilm Wako Pure Chemical) at 4°C for 2 h. Beads were washed twice with buffer A, twice with 1 : 4 mixture of buffer A and buffer B (25 mM Tris pH 7.4, 20 mM imidazole, and 0.1% Nonidet P-40), and finally twice with buffer B. Proteins were eluted from the beads by the addition of SDS loading dye containing EDTA and subjected to immunoblotting.

Identification of ubiquitination sites by mass spectrometry

HEK293FT cells were transfected with HA-BRD8 (pCAGGS-HA BRD8). Thirty-six hours after transfection, the cells were treated with MG132 (8 μM) overnight and harvested. The cells were washed with PBS and suspended in 8M urea containing Benzonase (Novagen, Madison, WI). Trypsin-digested peptides with ubiquitination-derived diglycine remnants were purified using PTMScan HS Ubiquitin/SUMO Remnant Motif (K-ε-GG) Kit (Cell Signaling Technology), as recommended by the manufacturer. The enriched peptides were analyzed by Orbitrap Eclipse Tribrid mass spectrometer with FAIMS Pro interface (Thermo Fisher Scientific), which was connected to Vanquish Neo UHPLC system (Thermo Fisher Scientific). Peptide identification was performed using SEQUEST HT algorithm in Proteome Discoverer Software (v2.5) (Thermo Fisher Scientific) based on the statistical criterion of a false discovery rate <1%.

NanoBRET PPI analysis

Interaction between BRD8 and histone H4 was assessed using the NanoBRET Nano-Glo Detection Systems according to the manufacturer's instructions (Promega). NanoLuc-BRD8, NanoLuc-BRD8ΔB, NanoLuc-BRD4, NanoLuc-BRD4ΔB, and histone H4-HaloTag fusion plasmids were prepared using In-fusion cloning (In-Fusion HD Cloning Kit, Takara Bio) or restriction enzyme-based methods. (Table S8). HCT116 cells were seeded on 6- well plates at a density of 8×10^5 cells/well and allowed to adhere overnight. Histone H4-HaloTag plasmids were introduced into the cells in combination with NanoLuc fusion plasmids (HaloTag/NanoLuc ratio of 1 : 1) using FuGENE HD (Promega). After 24 h of post-transfection, the cells (4×10^4 cells) treated with vehicle (DMSO) or NanoBRET 618 fluorescent ligand (100 nM) were transferred into 96-well plates, and further incubated for 8 h at 37°C. Donor emission (460 nm) and acceptor emission (618 nm) were measured using GloMax Discover System (Promega) or CLARIOstar Plus (BMG Labtech, Ortenberg, Germany) after the addition of NanoBRET Nano-Glo substrate. To determine whether bromodomain and extraterminal domain (BET) inhibitors affect the interaction between BRD8 and histone H4, JQ1 (Cayman, Ann Arbor, MI, USA) was added into the culture media at a concentration of 500 nM for 18 h. The raw BRET ratio was determined as a ratio of the acceptor emission value to the donor emission value. The ΔBRET ratio was calculated as the difference in the BRET ratio between cells treated with and without ligand.

Reporter assay for measuring Wnt signaling activity

TOPflash and FOPflash reporter plasmids were purchased from Merck. The reporter and pRL-null (Promega) plasmids were transfected into HCT116 and SW480 cells with control or BRD8 siRNAs using Lipofectamine 2000 (Thermo Fisher Scientific). Forty-eight hours after transfection, reporter activities were measured using the PicaGene Dual Sea Pansy Luminescence Kit (Fujifilm Wako Pure Chemical) and Centro XS LB 960 luminometer (Berthold Technologies, Bad Wildbad, Germany).

RNA-seq analysis

HCT116 and SW480 cells were transfected with control siRNA, BRD8 siRNAs (#6 and #36), or TIP60 siRNAs (#2 and #11) at a concentration of 10 nM using Lipofectamine RNAiMAX (Thermo Fisher Scientific), and maintained for additional 48 h. Total RNA was extracted from the cells using the RNeasy Plus Mini kit (Qiagen, Valencia, CA, USA), and quality of RNA was assessed using the Agilent Bioanalyzer device (Agilent Technologies, Santa Clara, CA, USA). All samples that have a RIN (RNA Integrity Number) value of more than 9.0 were subjected to library preparation. RNA-seq libraries were prepared with 100 ng of total RNA using an NEBNext Ultra II Directional RNA Library Prep Kit (New England Biolabs, Ipswich, MA, USA) according to manufacturer's instructions. The libraries were sequenced with 60 bp single-end reads to a depth of at least more than 10 million reads per sample on the HiSeq2500 platform (Illumina, San Diego, CA, USA). Sequencing data were analyzed by a standard RNA-seq analytical pipeline. Briefly, the sequencing data were aligned to human genome (hg38) using STAR aligner (v2.7.3a).[51] RSEM (v1.3.3)[52] was used to obtain the raw gene counts from the read alignments. The DESeq2 package (v1.26.0)[53] was used to normalize the read count data and test for differential gene expression.

Over-representation analysis (ORA)

A biological significance of the expression data was assessed by over-representation analysis. Differentially expressed genes by either BRD8 or TIP60 siRNAs were subjected to MSigDB GO (biological process, cellular component, and molecular function) and KEGG pathway analyses. Gene sets with FDR q-value <0.05 were considered significant.

Extraction-of-expression modules analysis

To analyze the association between subsets of BRD8 or TIP60 target genes and clinical information, we performed extraction-of-expression modules (EEM) analysis (Figure S5A, https://github.com/atusiniida/EEM2. 0).[28] The transcriptome data (FPKM with Upper Quantile normalization) of the TCGA-colon adenocarcinoma (COAD) patients (n = 456) were downloaded from Genomic Data Commons Data Portal (https://portal.gdc. cancer.gov/). Each of the FPKM values was log2-transformed after addition of one. We applied EEM to the log2-transformed gene expression data with pre-defined gene sets, e.g., the set of 421 down-regulated genes in BRD8-KD cells. EEM identified a coherently expressed gene subsets, i.e., expression module, in a predefined gene set (Figure S5B). For each expression module, we obtained the expression-module score for each patient as the average of z-scored expression values of genes in the expression module. Among the 456 cases of TCGA-COAD, the prognostic information was available for 453 patients, who were then divided

into those with higher (≥0) and with lower (<0) expression-module scores. Overall survival curves were plotted according to the Kaplan–Meier method. The generalized log-rank test was used to compare the survival curves between the two groups. A p value of 0.05 or less was considered statistically significant.

ChIP-seq analysis

HCT116 and SW480 cells were cross-linked with 1% formaldehyde for 10 min at room temperature and quenched with 125 mM glycine. Chromatin extracts were sheared by micrococcal nuclease digestion (New England Biolabs), and protein-DNA complexes were subsequently immunoprecipitated with 2 µg of anti-BRD8 polyclonal antibody (Sigma-Aldrich Cat# HPA001841, RRID:AB_1845438) bound to Dynabeads Protein G (Thermo Fisher Scientific). After de-crosslinking (65°C, overnight), samples were treated with RNase A (Merck) for 2 h at 37°C and Proteinase K (Merck) for 30 min at 55°C. DNA was purified by the conventional DNA extraction method, and then subjected to the preparation of sequence library. DNA concentrations of input and ChIP samples were measured using Qubit dsDNA HS Assay kit (Thermo Fisher Scientific). One ng of DNA and NEBNext Ultra II DNA Library Prep kit (New England Biolabs) were used for the preparation of libraries according to the manufacturer's instruction. The libraries were sequenced with 150 bp paired-end reads on the DNBSEQ-G400RS platform (MGI Tech, Shenzhen, China). The raw sequencing reads were analyzed for quality using FastQC and then aligned to human genome (GRCh38) using Bowtie2 (v2.4.1).[54] Peak calling followed by assignation of peaks to genes was performed using MACS2 (v3.6)[55] and HOMER (v4.11).[56] Peaks with *q*-value <0.05 were considered significant. Overlapping peaks in ChIP-seq data of HCT116 and SW480 cells were identified using the mergePeaks function in the HOMER software. Known motif analysis were performed using the HOMER findMotifsGenome function, with the settings in a 200 bp range surrounding peak centers for finding both primary and co-enriched motifs.

To validate the results of ChIP-seq analysis, ChIP followed by quantitative PCR (ChIP-qPCR) was performed as described previously.[57] Non-immune rabbit IgG (Santa Cruz Biotechnology, Dallas, TX, USA) was used as a negative control. The precipitated DNAs were subjected to qPCR analysis using sets of primer encompassing genomic region with peak. Amplification of exon 1 of the glyceraldehyde-3-phosphate dehydrogenase (*GAPDH*) gene was used as a negative control. The primer sequences used are listed in Table S8.

Establishment of BRD8-knockout cells

Guide RNA against BRD8 was designed using the CRISPRdirect (https://crispr.dbcls.jp/). A double-strand DNA with 4-bp overhangs at both ends was cloned into *Bbs*I site in pSpCas9(BB)-2A-GFP vector (PX458, Addgene). HCT116 and SW948 cells were transfected with PX458-BRD8-gRNA using FuGENE6 (Promega). The cells were cultured for an additional 24 h, and GFP (gRNA/Cas9)-positive cells were isolated by FACS (FACSAria, Becton Dickinson). Subsequently, single-cell cloning was performed, and clones lacking BRD8 expression (BRD8-KO) were determined by immunoblotting with anti-BRD8 antibody. In addition, disruption of the *BRD8* gene at the target locus in BRD8-KO clones was confirmed by TA cloning (Thermo Fisher Scientific) and Sanger sequencing. The primer sequences used for the amplification and sequencing are shown in Table S8.

QUANTIFICATION AND STATISTICAL ANALYSIS

Data are presented as the mean ± SD. The unpaired t-test was used when two independent groups were compared. For groups larger than two, statistical analysis was performed using one-way analysis of variance (ANOVA) with Dunnett's or Turkey's post hoc test. These statistical analyses were performed using the BellCurve for Excel software (Social Survey Research Information, Tokyo, Japan) or R version 3.6.3. In RNA-seq and ChIP-seq analyses, significance level was set at a Benjamini-Hochberg FDR-adjusted p value (i.e., *q*-value) of less than 0.05.